MECHANICAL BEHAVIOUR OF RUBBER BEARINGS WITH LOW SHAPE FACTOR

Alessandra Orfeo[1*], Enrico Tubaldi[1], Alan H. Muhr[2], Daniele Losanno[3]

[1]Department of Civil and Environmental Engineering, University of Strathclyde, Glasgow, UK

alessandra.orfeo@strath.ac.uk (*corresponding author), enrico.tubaldi@strath.ac.uk

[2]Tun Abdul Razak Research Centre-TARRC, Hertford, UK

ahmuhr@googlemail.com

[3]Department of Structures for Engineering and Architecture, University of Naples Federico II, Napoli, Italy

daniele.losanno@unina.it

ABSTRACT

This study investigates the mechanical behaviour of elastomeric bearings with a low shape factor (LSF). Such bearings can offer an effective solution for three-dimensional seismic isolation of structures, that is, isolation in vertical as well as horizontal directions. They could also be employed for developing low-cost isolation systems for developing countries due to their reduced weight and manufacturing cost.

The first part of the study describes tests carried out at Tun Abdul Razak Research Centre (TARRC) on low-damping rubber double-shear test pieces and LSF bearings. The material tests are used to inform the development of a finite element (FE) model of the bearings, which is validated against the bearing test results. It is shown that the proposed FE model can be used to describe accurately the global non-linear horizontal force-displacement behaviour of the compressed bearings, while providing an insight into the local distribution of stresses and strains. It can also be used to investigate the bearing response under boundary conditions that differ from the one considered in the tests.

The second part of the study illustrates the numerical simulations of shaking table tests carried out at the University of Naples Federico II on a structural prototype mounted on the low-damping LSF bearings. Useful insights are provided into the effect of the vertical bearing flexibility on the response and the attainment of critical conditions of zero tangent horizontal stiffness under horizontal displacements.

KEYWORDS Seismic isolation, rubber bearings, low shape factor, shaking-table tests, 3D finite element analysis

1. INTRODUCTION

Seismic isolation is a technique aimed at protecting structures from earthquakes by shifting their fundamental frequency away from the undesirable frequencies of seismic ground motions. Laminated rubber bearings are widely used in the isolation system. They consist of multiple layers of rubber vulcanized to steel reinforcing layers that produce a vertically stiff but horizontally flexible isolator [1]. A non-dimensional parameter usually

employed to characterize the geometry of these bearings is the primary shape factor, S. This defines the ratio of the loaded area to the area free to bulge for an individual rubber layer [2-3]. Common values of S for laminated rubber seismic isolators are in the order of 10-20. This is to enhance the critical load capacity of the bearings, and to minimise rocking motion in isolated structures by providing a high vertical stiffness, while maintaining a low horizontal stiffness. Such bearings have been widely deployed and thoroughly studied, and most design criteria in publications and Standards are focussed on bearings of this type. However, high S values, ranging from 10 to 30, result in a large number of steel plates, resulting in significant weight of the bearings, and generally high production and installation costs. At the same time, the high vertical stiffness of the bearings yields high vibration frequencies of the isolated structure in the vertical direction.

Vibration isolation is a technique for protecting structures from ground-borne vibration, for example produced by underground trains. Laminated rubber-steel bearings have been used as structural vibration isolators from the 1960s [1,4,5]. In vibration isolation systems the objective is to provide an approximately isotropic stiffness, vertical and horizontal, with natural frequencies of approximately 5Hz, so as to attenuate ground-borne vibrations in the audible range (>15Hz). The success of such systems was the inspiration for developing seismic isolation systems based on rubber bearings. However, it was quickly realised that designing for an approximately isotropic system would be impractical for seismic isolation, since most damage is associated with a predominant low frequency horizontal content, typically in the range between 1Hz and 10Hz, calling for an isolation frequency of around 0.5Hz [1,4]. While it proved possible to design laminated bearings giving such a low horizontal natural frequency for typical column loads, for a linear spring with a vertical natural frequency of f = 0.5Hz, the vertical deflection would be of the order of $g/(2\pi f)^2 \approx$ 1m, and thus completely impractical. Fortunately, typical superstructures are far from isotropic in modal frequencies, only the horizontal structural modes having low enough modal frequencies to be dangerously excited by the seismic motion, and so the standard base isolation system was developed to have a horizontal period of about 0.5Hz, and to be nearly rigid vertically, to minimise rocking. Such a “two dimensional” isolation system provides good protection to the superstructure, however, it does not provide isolation from significantly higher frequency vertical ground motion, whether seismically or otherwise induced, that might cause undesirable excitation of vertical modes of superstructure or contents. This could be the case for critical facilities such as nuclear power plants or hospitals hosting sensitive equipment, for example. Moreover, the encouragement of some rocking in the first horizontal mode, by lowering vertical stiffness, has also the potential to lower its modal frequency and hence might also significantly improve isolation from the horizontal component of seismic excitation.

It is noteworthy that in the early stages of development of seismic isolation bearings, some researchers investigated the possibility of employing low shape factor (LSF) rubber bearings, ranging from 0.5 to 5, as a way to achieve an economic three-dimensional (3D) isolation of structural systems. The first example of a structure isolated using rubber bearings, the Pestalozzi school built in 1969 in Skopje (Macedonia), was realized using unreinforced rubber blocks, with S=0.5, assuming no lateral slip on the pedestals. These blocks exhibited significant lateral bulging under the weight of the building and were eventually replaced with high shape factor steel-reinforced bearings [6]. A base-isolated laboratory building realized in Kajima Corporation Technical Research Institute [7] was one of the earliest applications of LSF bearings (S=2.5). The two-story reinforced concrete building was supported on eighteen bearings, and auxiliary steel bars provided damping. The aim was to provide 3D seismic isolation from earthquakes as well as ambient ground vibrations and the effectiveness of the system was shown in the laboratory testing. Aiken et al. [8] designed a 3D isolation system for a liquid metal reactor building; their study involved the design and testing of bearings with shape factor S=5.4, made from different types of rubber material, and the development of an analytical bearing model. For them, "low shape factor bearings" corresponded to those designed to achieve both vertical and horizontal isolation. However, the dynamic response of the structure supported on such bearings was not investigated in detail, either experimentally or theoretically.

A solution investigated by many researchers to reduce the weight and cost of isolators consists of the replacement of steel plates with fiber reinforcement materials [9-12]. Fiber-reinforced elastomeric bearings have also been proposed to provide 3D isolation, since they have a lower vertical stiffness in comparison to an equivalent steel-reinforced elastomeric bearing [5].

Kelly and Lee [13] analysed the existing literature about 3D seismic isolation and explored theoretically the dynamics of 3D isolation systems and the presence of rocking modes for low values of the bearing vertical stiffness. Warn and Wu [14] showed with the aid of numerical simulations that buildings isolated on LSF bearings could experience minor non-structural damage following a major earthquake event. Yabana et al. [15] carried out tests to evaluate the mechanical characteristics and the performance of rubber bearings with a shape factor of 4.2, highlighting the effect of decrease of the rubber thickness, caused by the vertical pressure, on the bearing horizontal stiffness, and the high displacement capacity (shear strains>500%), which is similar to that of more conventional bearings. Zhou et al. [16] and Okamura et al. [17] both considered the application of LSF bearings to 3D isolation of modern nuclear facilities. Cilento et al. analysed results from an extensive experimental campaign to investigate the effectiveness of isolating a structure with LSF bearings [18].

In the last decades, several studies investigated the mechanical behaviour of elastomeric bearings, and various models were developed for describing their response under horizontal loading or combined vertical and horizontal loading (see e.g [3,19, and 20-28]). These models were successfully employed to evaluate the seismic performance of structures isolated with rubber bearings, see e.g. [29-31]. However, most of the bearing models developed thus far have been validated against tests on high shape factor bearings, and they do not account for important effects such as the reduction in height and the increase in plan area due to bulging of the elastomer under compressive load, which affect significantly the response of LSF bearings. Attempts were made by Stanton and Roeder [32,33], Shapery [34,35] and Muhr [36] to include such effects in bearing models, in order to extend their applicability to the LSF case, but more experimental tests are needed to validate these models.

Recently, some works have investigated experimentally and numerically the behaviour of LSF bearings, by mainly focusing on the compressive response. Gu et al. [37] carried out comprehensive tests on high damping rubber bearings with LSF, evaluating their behaviour in terms of vertical and horizontal stiffness, and equivalent damping ratio. They also proposed a corrected calculation of the vertical stiffness to provide a better agreement with the experimental results. Ren et al. [38] carried out both experimental and numerical investigations on the compressive behaviour of LSF lead-rubber bearings, demonstrating that differently from the case of high shape factor bearings, the axial load has a non-negligible effect on their compressive stiffness.

The few studies [13,14] that have investigated numerically the dynamic behaviour of structures mounted on LSF bearings are based on oversimplified descriptions of the bearings, e.g. using uncoupled spring elements for the various directions. Thus, an in-depth analysis of the behaviour of LSF bearings and of structures mounted on them, using experimental testing and advanced numerical modelling, is needed.

This paper aims to further explore the LSF concept in rubber bearings through the development of an advanced finite element (FE) modelling strategy for these isolation devices. The first part of the paper focuses on the bearing behaviour, using the results of double shear tests on rubber pieces and quasi-static tests on rubber bearings under compression and shear displacements carried out by Tun Abdul Razak Research Centre (TARRC). These tests are simulated in Abaqus [39] using a 3D modelling approach for the LSF bearings, with alternative constitutive laws for the rubber stress-strain behaviour based on the double shear test results. The advanced numerical modelling approach is used to achieve a deeper understanding of the mechanical behaviour of LSF bearings under combined axial and horizontal loads, and in particular to investigate the resulting local distribution of stress and strain throughout the rubber. It is noteworthy that these quantities are relevant for assessing the likelihood of local failure (e.g. debonding, and splitting in the rubber along the peak of the bulge),

and that this is particularly important for LSF bearings, which may exhibit debonding problems due to high shear stresses at the outer edge of the shim-rubber interface.

In the second part of the paper, the 3D bearing model is used for simulating shaking table tests carried out at the Department of Structures for Engineering and Architecture of University of Naples Federico II on a prototype base-isolated building with LSF bearings under a horizontal seismic input. The tests induced high displacements at the isolation system level, and significant variations of vertical forces. The simulation allows characterization of the complex bearing behaviour under dynamic loadings, involving significant coupling between the horizontal and vertical response.

It is noteworthy that although analysing an entire isolated structure with 3D FE modelling [40] is feasible, it is computationally too expensive for routine use. Here, this modelling strategy is used to shed light on the local behaviour of the rubber layers arising due to the application of external loading, for investigating the mechanical behaviour under loadings not considered experimentally but potentially encountered in real applications, and for checking the attainment of limit state conditions during the design stage [41]. It can also be used to calibrate and validate simplified modelling approaches for describing the bearing mechanical properties [32-36].

2. MATERIAL AND BEARING TESTS

This section describes first the tests carried out at TARRC to characterize the mechanical behaviour of the LSF bearings with low damping rubber. The tests include those on double shear test pieces for the characterization of the material behaviour and those on the compressed bearings under shear loading. Subsequently, these tests are simulated using a 3D finite element analysis approach. Although bearings manufactured with a high damping compound were also tested at TARRC, this study considers only the bearings made with the low damping rubber compound. This choice is motivated by the fact that low damping rubbers have a relatively simple constitutive behaviour, allowing the focus to be on the effects of finite strains and geometrical nonlinearity, arising from the combination of axial loads and horizontal displacements. The bearings made with the high damping compound would be characterized by a much more complex mechanical behaviour, affected by Payne effect, stress-softening, and potential heating of rubber upon repeated cycling (see e.g. Tubaldi et al. [28], Ragni et al. [42]).

2.1 Experimental Tests

Double-shear cylindrical test pieces made of lightly filled natural rubber compound were subjected at TARRC to harmonic displacement histories. The test pieces consisted of two rubber layers hot-bonded to metal parts as

shown in Fig. 1a. The thickness of each layer was 6mm and the diameter 25mm. Double shear tests were performed under sinusoidal shear displacement histories with a frequency of 0.5 Hz. The samples were preconditioned (i.e. non virgin). Nevertheless, the stress-softening effects [28,42] are not significant since the compound is a low damping and essentially unfilled natural rubber, and for the same reason the effect of the temperature rise in the rubber upon repeated cycling is negligible. Fig. 1b shows the results of the tests in terms of variation of the secant shear modulus G with the maximum nominal shear strain γ_{max}. The nominal shear strain γ is defined as the ratio between the shear displacement and the rubber height of a single layer, whereas the secant shear modulus G is evaluated as the ratio between the maximum nominal shear stress τ_{max} (obtained by dividing the maximum shear force by the cross-sectional area of the rubber sample) and γ_{max}, under the assumption of uniformly distributed shear strains. It can be observed that G assumes values in the range between 0.62 MPa and 0.47 MPa, reducing slightly for increasing values of γ_{max}. Fig. 1c also shows the variation of the equivalent damping ratio [43] with the strain amplitude. The damping ratio is generally very low, as expected for this type of rubber compound, and increases slightly for increasing γ_{max} values.

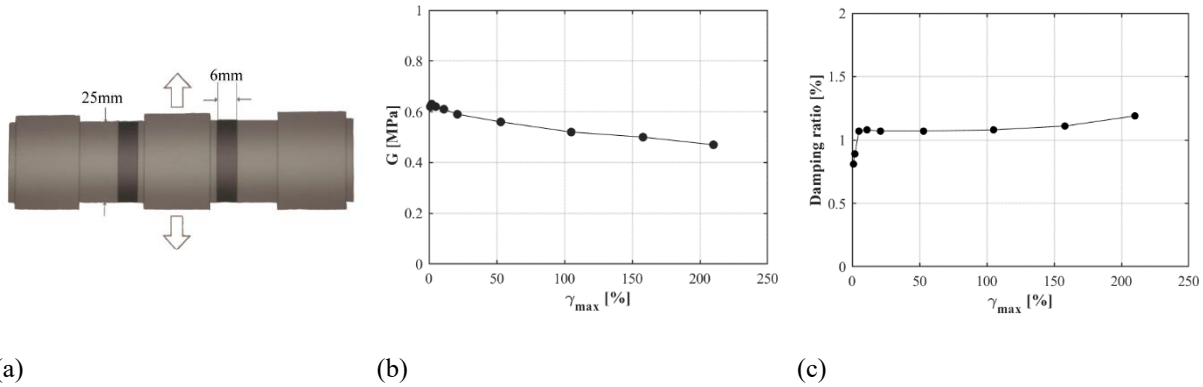

(a) (b) (c)

Fig. 1 – (a) Double shear test piece geometry, (b) Secant shear modulus vs. maximum shear strain, (c) Equivalent damping ratio vs. maximum shear strain

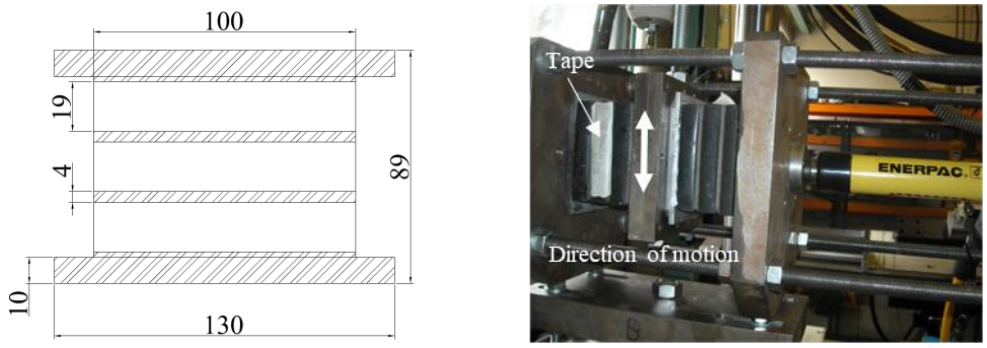

Fig. 2 – (a) Bearing geometry, (b) Double shear test set-up: two identical bearings mounted in the test jig, the external plates are fixed after the application of compression load and the central plate is free to move along the direction perpedicular to the compression load.

Fig. 2a illustrates the laminated bearing considered in the tests and Fig. 2b shows the bearings in the test jig. These prototype bearings were designed to achieve target horizontal and vertical natural periods respectively equal to 0.92s and 0.25s for the scaled prototype. They consist of three layers of rubber 19mm thick and sides 100x100 mm, vulcanised and simultaneously hot-bonded (using the Chemosil 211/220 system [67], as also used for the double shear test piece of Fig. 1a) to steel plates (nominal thickness 2mm) on their major faces, designed to achieve a shape factor S=1.32. Loctite 638 [68] retaining compound was used to bond the three rubber–steel laminates together, on the two internal steel to steel interfaces. Steel end plates 130mm x100mm, with thickness 10 mm, were bonded to the end steel faces of the 3-layer bearing using Araldite standard epoxy adhesive. Four bearings were built and tested at TARRC; a pair of bearings was subjected simultaneously to static compression and dynamic shear loading in a double shear configuration. A hydraulic jack was used to apply a compression load to the bearings to simulate gravity loads, whereas the shear displacements were imposed by a Dartec uniaxial servohydraulic actuator. The compression load was increased up to the desired level, and subsequently the external plates were locked tightening bolts on both sides (see Fig. 2b) before applying a shear displacement through the central plate. The testing sequence consisted of two cycles of sinusoidal displacement at increasing shear strain amplitudes [18,44]. It is worth observing that during both these tests and the shaking table tests described in Section 3.1, no failure in terms of rubber-to-metal bonding was observed, despite the bearings having been subjected to relatively high horizontal displacements. Similarly in other studies on LSF bearings [15] no debonding was observed, for bearings subjected to higher compression and shear deformations. Nevertheless, some technological solutions may be employed to minimize the debonding risk, e.g. using fillets [45]. The test setup considered to characterise the shear response of the bearings under different compressive loads is somewhat different from that employed in studies in the literature, where the compressive load rather than the compressive displacement is fixed. Obviously, the approach followed is cheaper and also easier, but care must be paid in interpreting the obtained results and comparing them to those in the literature. Nevertheless, the obtained results are still useful for model validation and the shear response under small deflections is the same regardless of the boundary condition, as discussed below.

The secant shear stiffness is calculated from the hysteresis loops obtained from the shear tests, and can be defined based on values of peak force F_{max} and peak displacement d_{max} as follows:

$$k_s = F_{\max} / d_{\max} \tag{1}$$

Fig. 3a shows the shear stiffness values of one bearing for increasing nominal shear strains, defined by the ratio between peak displacement and the total rubber thickness, obtained under a compressive displacement

corresponding to 19kN (i.e. a pressure of 1.9 MPa) at zero shear deformations. It can be noted that contrary to what was observed in the case of double shear tests under zero compression, the secant shear stiffness first reduces slightly for increasing nominal shear strains, and then it increases. This behaviour is in contrast with the existing literature on elastomeric bearings, showing a reduction of the horizontal stiffness under increasing horizontal displacements [46,47]. This is due to the fact that the vertical load in the bearings (which was not measured during the experiments) is expected to decrease with increasing lateral displacement. The Payne effect (i.e., the decrease of stiffness for increasing deformation, typical of HDNR compounds [19,28,42]) cannot explain this behaviour since the rubber compound incorporates very little filler. Fig. 3b illustrates the equivalent damping ratio of the bearing at various shear strains. It is interesting to observe that the equivalent damping ratio of the device (between 2% and 3%) is in general significantly higher than that of the rubber compound (about 1%) and it increases for increasing compression levels. This phenomenon was observed in experiments reported by Thomas [48] and also acknowledged by Koh and Kelly [23] and Raithel and Serino [49], who noted that when viscoelasticity is included in their theory the compression load increases the phase difference between the horizontal force and the horizontal displacement, thus increasing the energy dissipation per cycle. Despite this increase, the damping ratio of the bearings is still quite low and in real applications a higher value may be desirable to control the displacement demand. This could be achieved by using auxiliary damping devices, e.g. viscous dampers or steel bar dampers [7,50] or by using more dissipative compounds. The second solution is preferable since it would not reduce the cost benefits of the LSF bearings. It is noteworthy that similar bearings were also made using a high damping NR compound and, due to the augmentation of damping through the high compressive load, were very effective in the shaking table tests in controlling the displacements, albeit at the expense of higher drifts and accelerations in the superstructure (Fig 14, Cilento et al. [18]), though are not further discussed here.

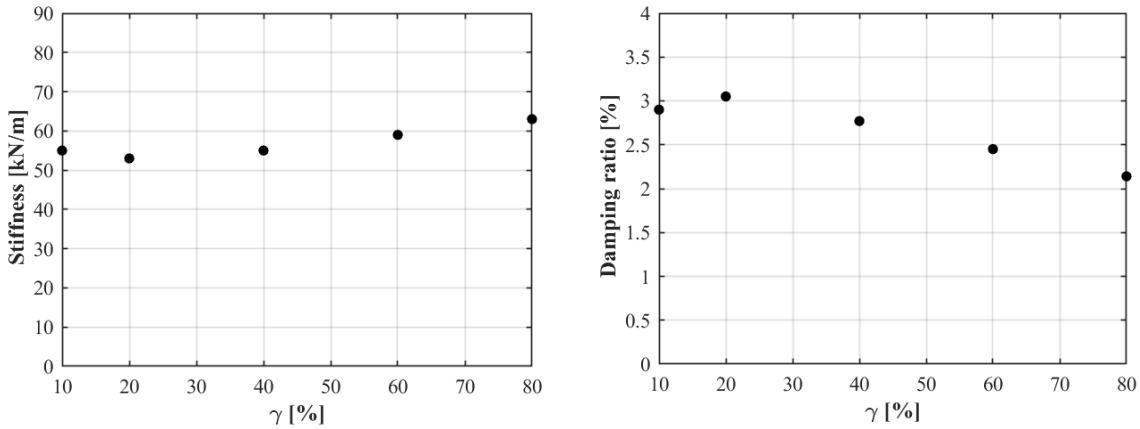

(a) (b)

Fig. 3 – (a) Bearing horizontal stiffness vs. nominal shear strain, (b) Damping ratio vs nominal shear strain. The compressive strain is held constant during shear, at a value corresponding to 19kN force for zero shear strain.

2.2 3D Numerical Model

This subsection describes the 3D numerical models developed in Abaqus [39] to simulate the tests on the double shear pieces and the elastomeric bearings, to provide an insight into the local stresses and strains throughout the double shear pieces and the elastomeric bearings, to investigate the influence of axial compression on the horizontal response and to estimate the critical load.

2.2.1. Constitutive models

In the models, the rubber is described using a hyperelastic constitutive material. Hyperelastic materials are defined by the strain energy potential *W,* the strain energy stored in the material per unit of reference volume as a function of the strain in the material. Three alternative constitutive relationships are used and compared in this study, namely the neo-Hookean, Ogden and Yeoh models [51].

Assuming an incompressible material, the Ogden strain energy function depends on the three principal stretches λ_1, λ_2, λ_3 and $2N$ material constants, i.e. the hyperelastic parameters, μ_i and α_i, according to the following expression:

$$W = \sum_{i=1}^{N} \frac{\mu_i}{\alpha_i} \left(\lambda_1^{\alpha_i} + \lambda_2^{\alpha_i} + \lambda_3^{\alpha_i} - 3 \right) \tag{2}$$

where N is the number of terms that constitute the strain energy density function, chosen to be 1 in this study.

The Yeoh and neo-Hookean strain energy potentials are derived from the reduced polynomial strain energy potential that is a function of only the deviatoric strain invariant I_1 and has the following expression:

$$W = \sum_{i=1}^{N} C_{i0} \left(I_1 - 3 \right)^i \tag{3}$$

where C_{i0} are material parameters. The Yeoh and neo-Hookean form are obtained for a number of terms N equal to 3 and 1, respectively. The values of material parameters μ_i, α_i and C_{i0} in the Eq. (2) and (3) can be obtained from the double shear experiments described in the previous section. These parameters have been calibrated by considering the simple shear secant modulus-strain relation for all three material models, assuming a homogeneous state of simple shear strain within the cylindrical rubber pieces (Fig. 1a). The relation between principal stretches and amount of shear, is given by [51]:

$$\lambda_1 = \lambda = \sqrt{1 + \frac{\gamma^2}{2} + \gamma \sqrt{1 + \frac{\gamma^2}{4}}}; \; \lambda_2 = \lambda^{-1}; \; \lambda_3 = 1; \; \lambda\text{-}\lambda^{-1} = \gamma \tag{4}$$

The principal first invariant as a function of the amount of shear is expressed as follows:

$$I_1 = \gamma^2 + 3 \tag{5}$$

As developed by Rivlin [52], the relation between shear stress and γ is:

$$\tau = 2\left(\frac{\partial W}{\partial I_1} + \frac{\partial W}{\partial I_2}\right)\gamma \tag{6}$$

Assuming the strain energy density depends only on I_1, then Eq. (6) gives:

$$\tau = \frac{\partial W}{\partial I} 2\gamma \tag{7}$$

The stress-stretch relation according to Ogden's model, Yeoh's model and the neo-Hookean model can be expressed respectively as follows:

$$\tau = 2\mu \frac{\lambda}{1+\lambda^2}\left(\lambda^{\alpha} - \lambda^{-\alpha}\right) \tag{8}$$

$$\tau = 2\gamma\left(C_{10} + 2C_{20}\gamma^2 + 3C_{30}\gamma^4\right) \tag{9}$$

$$\tau = 2\gamma C_{10} \tag{10}$$

where $2C_{10}$ in Eqn. (10) represents the rubber shear modulus.

The material parameters of the various constitutive models, found by fitting the parameters of these equations to the experimental double-shear test results, are shown in Table 1.

Table 1 Material parameters for the three hyperelastic material models

Model parameters	**C10 [MPa]**	**C20 [MPa]**	**C30 [MPa]**	**α [–]**	**μ [MPa]**
Ogden	-	-	-	1.42	0.61
Yeoh	0.3	-0.005	0.000311	-	-
neo-Hookean	0.292	-	-	-	-

The damping property of the rubber material is described in a simplified way by using a Rayleigh damping model, whose coefficients are calculated to provide a damping ratio of 1% in correspondence of the first and second vibration modes of the isolated system described in Section 3. The coefficient α for the mass matrix and the coefficient β for the elastic initial stiffness matrix are equal to 0.067926 and 0.00080, respectively.

2.2.2. Simulation of material characterisation tests

Fig. 4 describes the FE model of the double shear test. Since the double shear configuration has a plane of symmetry, only half of a single layer is modelled, in order to reduce the computational cost of the simulation, by imposing appropriate boundary conditions. The rubber layer is modelled using 8-node solid elements (C3D8H) with first-order hybrid formulation, which is recommended for incompressible materials [39]. The model

domain has been meshed employing only hexahedron elements, and avoiding excessive values of their aspect ratio in the central part. In the simulation, a sinusoidal load in the horizontal direction (i.e., x) is applied to the top reference point in a displacement control analysis and the bottom of the layer is fixed.

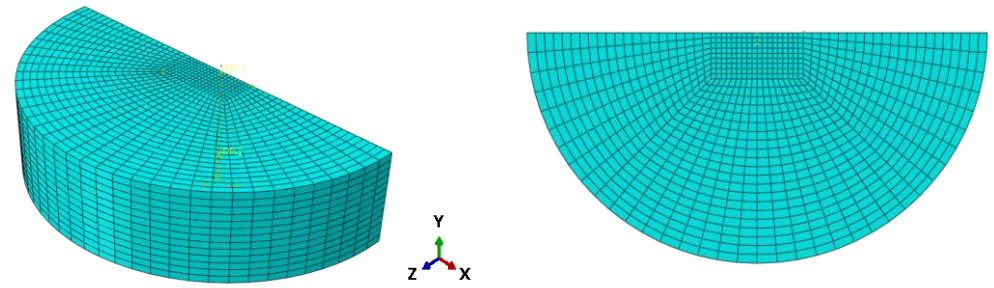

(a) (b)

Fig. 4 – FE model and meshing of the double shear test (a) 3D Perspective, (b) Top View.

Fig. 5a shows the distribution of shear stresses and strains in a vertical section along the diameter of the reference cylindrical layer, obtained using the Yeoh model under a shear displacement of 6 mm. This corresponds to a nominal shear strain of 100%. The local shear strains and stresses are quite uniformly distributed within the rubber layer and their values are very close to the nominal ones, apart from the areas close to the edges, where they are higher. This confirms that the state of deformation in this test configuration is nearly, but not exactly, “simple shear”, as also pointed out by others (e.g. Rivlin [52], Gregory et al [53]).

Fig. 5b compares the experimental force-displacement response with the response simulated using the Yeoh model. It is observed that the response is close to linear and that the model provides a good approximation of the experimental results. The value of the shear modulus for the neo-Hookean model that provides the best fit to the experimental results among various investigated values is 0.584MPa, corresponding to C_{10}=0.292 MPa. Fig. 6a reports and compares the shear stiffness values from both the experimental tests and the FE analyses results for different maximum shear strains. A good agreement between simulations and the test is found for all the investigated shear deformation amplitudes, apart from low values of shear strains. In general, using the Ogden and Yeoh constitutive relationship for the rubber yields the most accurate results, especially at high levels of shear strains. The neo-Hookean relationship provides a worse fit, because it is characterized by a reduced number of parameters compared to the other models and yields an almost linear response under simple shear strains (the slight departure from linear response is due to the strain field not being exactly simple shear). The estimates of the equivalent damping ratio of the rubber block obtained with the Yeoh constitutive model combined with Rayleigh damping for different levels of strain amplitude are shown in Fig. 6b, where they are compared with the corresponding values obtained experimentally.

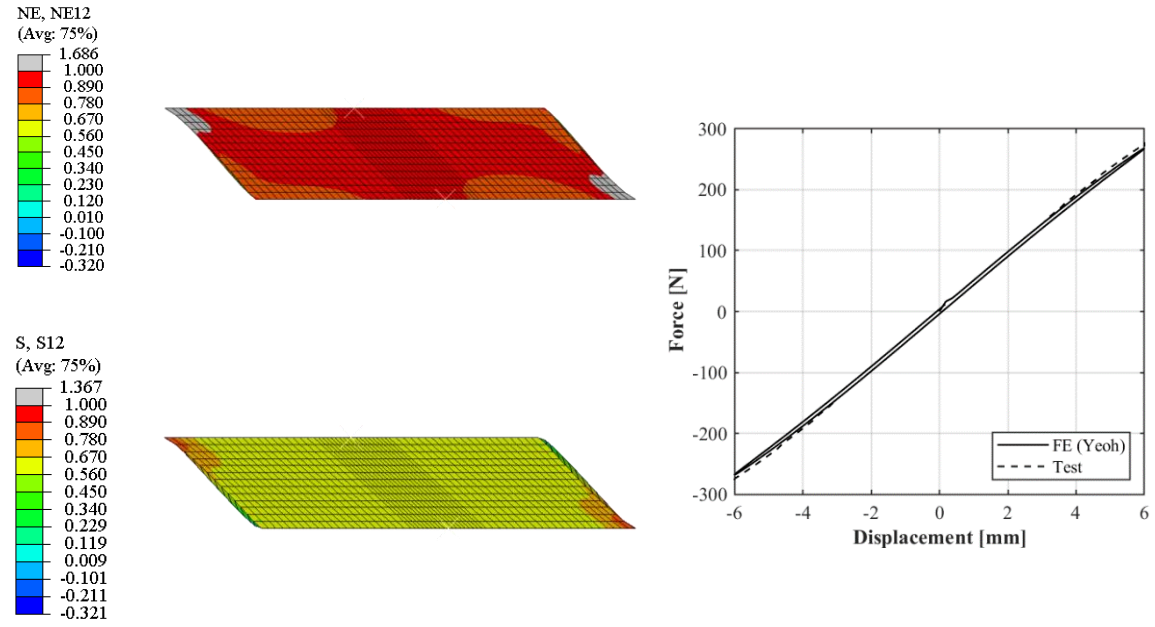

(a) (b)

Fig. 5 – (a) Contour plot of the shear strain (top) and stress (bottom) component within the rubber shear test piece, (b) Hysteresis loop of each rubber test piece for a nominal maximum shear strain of 100%

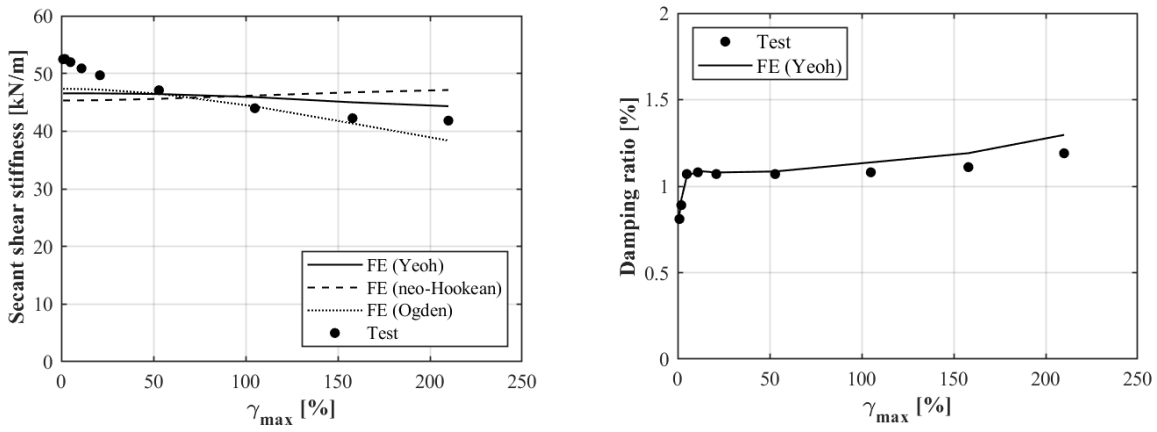

(a) (b)

Fig. 6 – Experimental and FE models' results of (a) Secant shear stiffness for different maximum shear strains, (b) Equivalent damping ratio for different maximum shear strains.

It is noteworthy that more advanced description of the damping, e.g. using a Prony series approach can also be used to capture the behaviour of low damping natural rubber with a simple fitting procedure described in Ahmadi et al's work [54]. However, in this paper the Rayleigh damping model has been employed because the agreement with experimental results is already good, considering that a relatively simple description of the damping is used for the rubber material.

2.2.3. Simulation of bearing tests

Fig. 7 illustrates the model of the LSF bearing, which is the same as those employed in the shaking table test, whose results are discussed in the next section. The intermediate steel shim plates and end plates are also modelled using C3D8H elements. The tie contact between steel and rubber layers of the bearing is expressed by

contact pair option available in Abaqus. The bottom anchor plate is fixed in all degrees of freedom and the top end plate is fixed against rotation but allowed to translate laterally and vertically. For the rubber layers, the constitutive models described in the previous section are employed, and the results shown are those obtained using the Yeoh constitutive model unless otherwise specified.

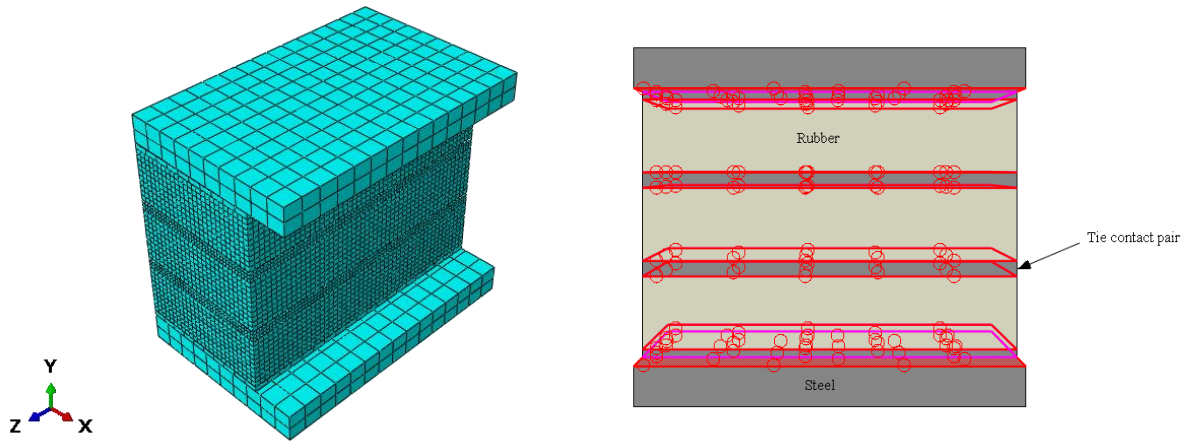

(a) (b)

Fig. 7 – Elastomeric Bearing: (a) Meshing, (b) Details of connections between various layers.

A vertical downward displacement is first imposed at the top plate, until a compressive load of 19kN is achieved, equal to the mean load per bearing under the gravity loads in the shaking table tests. Subsequently, two cycles of sinusoidal displacements are applied while preventing vertical motion and rotation of the top plate. Fig. 8a shows the force-displacement curves under the applied compressive load of 19 kN evaluated numerically with Yeoh, neo-Hookean and Ogden material models. Experimental data are not available for this stage of the test, nevertheless a similar behaviour is obtained with the different constitutive models. Fig. 8b illustrates the compressive load reduction due to the imposed sinusoidal shear displacement, which is due to the fact that the motion of the bearings in the axial direction is restrained. Fig. 8c shows the shear force-displacement behaviour of the bearing subjected to the applied load in combination with the maximum applied horizontal displacement obtained both numerically and experimentally. It can be observed that a similar shear behaviour is obtained among the different constitutive models. The relative error in terms of energy dissipation (area within the loops) obtained by the three models is only 20% when compared to the experimental result. Fig. 9 illustrates the deformed bearing during the tests. Fig. 10a shows the contour plot of true compressive and shear stresses, expressed in MPa, and the engineering compressive and shear strain for the bearing subjected to the compressive load of 19kN. Fig. 10b illustrates the stress and strain of the compressed bearing subjected to horizontal displacement of 46.48 mm, i.e. a nominal shear strain of about 80%. According to the legend notation, positive values indicate tensile stresses and strains, whereas negative values denote compressive stresses and strains. Although the bearing is globally subjected to axial compression and shearing, it can be

observed that local tensile stresses are developed within the bearing due to the bulging of the layers. Under compression, local tensile stresses and strains are concentrated along the bulging area, whereas the shear stress and strain are highest at the four edges, normal to the direction of horizontal deflection, close to the bonded surfaces. These observations are in line with the extensive theoretical investigation of Kelly [55], showing that high shear stresses appear at the corner of rubber pads, and with previous numerical studies on the response of elastomeric bearings [20]. Under horizontal displacement, compressive stresses and strains are distributed along a diagonal strip that corresponds to the compression strut, whereas tensile stresses are concentrated at top right and bottom left areas of the bearing [20]. It is also interesting to note that the steel reinforcing plates undergo bending deflections, but without experiencing yielding.

Table 2 reports the values of the nominal true axial and shear stresses and nominal strains obtained numerically. The stresses are evaluated by dividing the maximum vertical and horizontal reaction forces by the cross-sectional area of the bearing in the deformed configuration (i.e. the cross sectional area at which the compressive/horizontal displacement is applied), respectively. The strains are obtained by dividing the maximum vertical and horizontal displacements by the rubber bearing height, respectively. These values are compared with the maximum local stress and strain extracted from the contour plots of the numerical investigation, showing that the latter are significantly higher than the nominal values. The amplification percentage has been calculated as the difference between the nominal (from hand calculations) and local (from FE analysis) value divided by the nominal value.

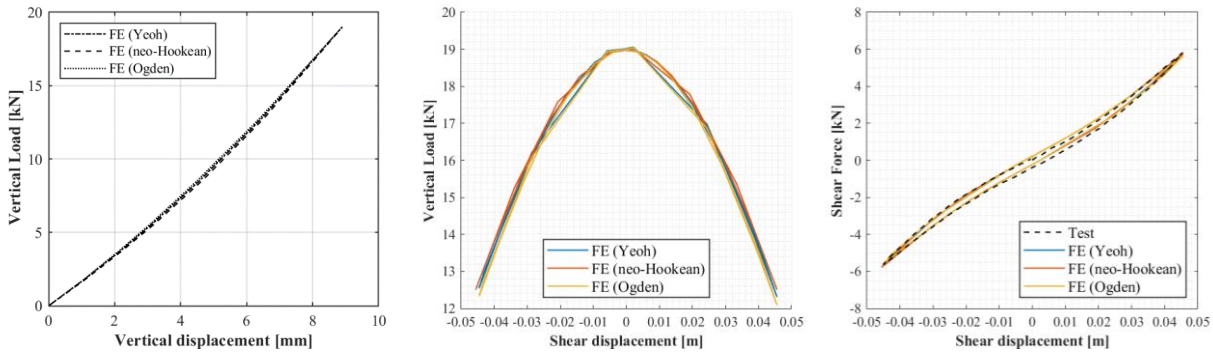

(a) (b) (c)

Fig. 8 – Force-displacement curves (a) Vertical load-displacement behaviour defined numerically using Yeoh, neo-Hookean and Ogden constitutive material models, (b) Numerical vertical force-shear displacement results (c) Numerical shear force-displacement results compared with the available experimental data.

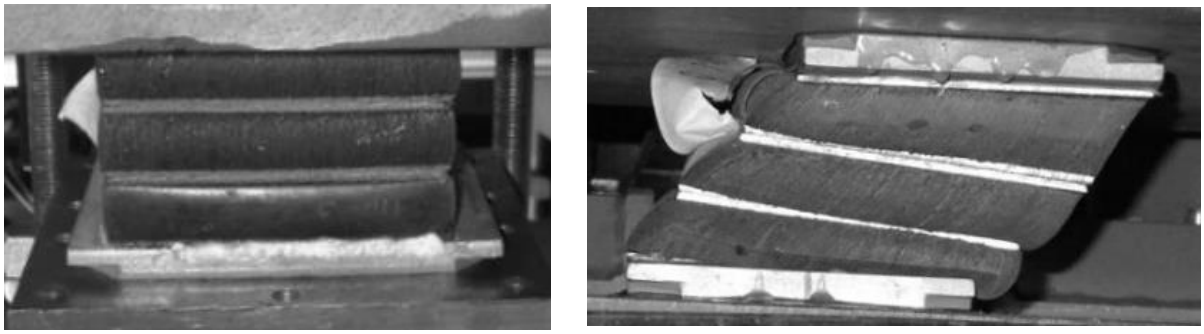

Fig. 9 – Deformed bearing under a compression load of 19 kN (left) and a combined compression load and shear displacement (right) during the experiment [44]

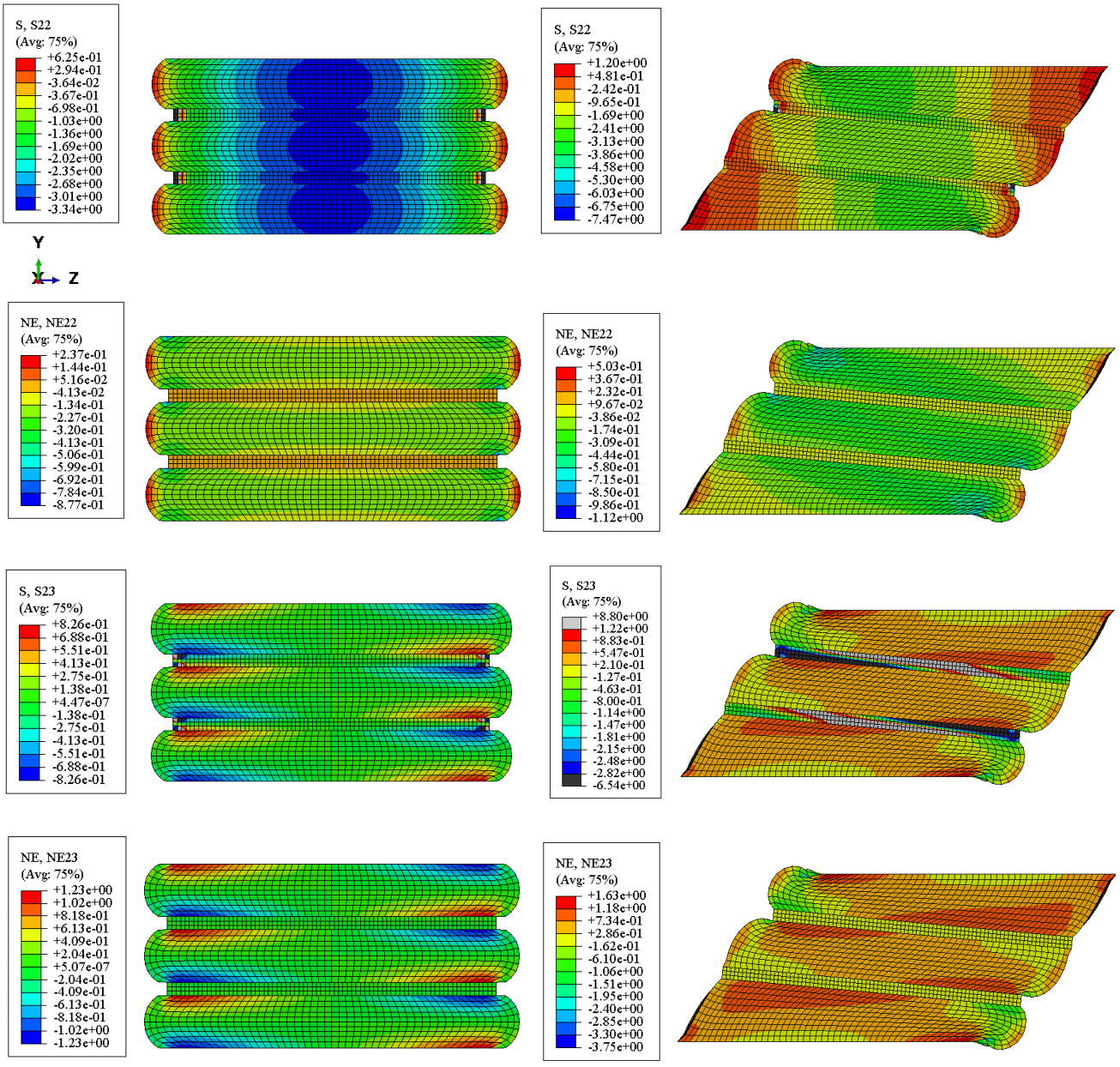

(a) (b)

Fig. 10 – Contour plot of compressive and shear Cauchy stresses (S) and compressive and shear engineering strain (NE) subjected to (a) Compressive load 19kN, (b) Compressive load 19kN in combination with horizontal displacement.

Table 2 Nominal and local stresses and strain values (First three columns related to Fig. 10a, last two related to Fig. 10b)

		True axial stress [N/mm^2]	Axial strain at max compression [-]	Shear strain at max compression [-]	True shear stress [N/mm^2]	Shear strain at max shear [-]
Nominal		2.25	0.16	0.80	0.68	0.8
Maximum local	neo-Hookean	3.54	0.85	1.20	3.58	3.20
	Yeoh	3.34	0.88	1.24	2.82	3.75
	Ogden	3.35	0.88	1.25	2.83	3.76
Δ% to nominal	neo-Hookean	57	445	50	427	300
	Yeoh	48	463	55	316	369
	Ogden	49	464	57	317	370

Fig. 11a shows the force-displacement loops obtained numerically using the Yeoh constitutive model and Rayleigh damping to simulate the results of the sinusoidal tests at different shear strain levels under the compressive load of 19kN. For small displacements, up to $\gamma = 40\%$, the bearing has an almost linear behaviour, with low energy dissipation achieved as illustrated both experimentally and numerically in Fig. 11c. Non-linear force-displacement behaviour is then observed as the displacement amplitude is increased. The horizontal secant stiffness of the bearing, obtained by dividing the base shear force by the maximum displacement at each incremental step, is plotted in Fig. 11b for each material model considered and compared against the experimental results. The increasing trend in secant stiffness is due to boundary conditions (i.e. reduction of axial force). In general, the experimental and numerical values are very close, except for low shear strains, for which the numerical model is more flexible. The equivalent viscous damping of the bearing is evaluated numerically and compared with the experimental results, as shown in Fig. 11d. Both experimental and numerical results show that with the increase of shear strains, the damping decreases.

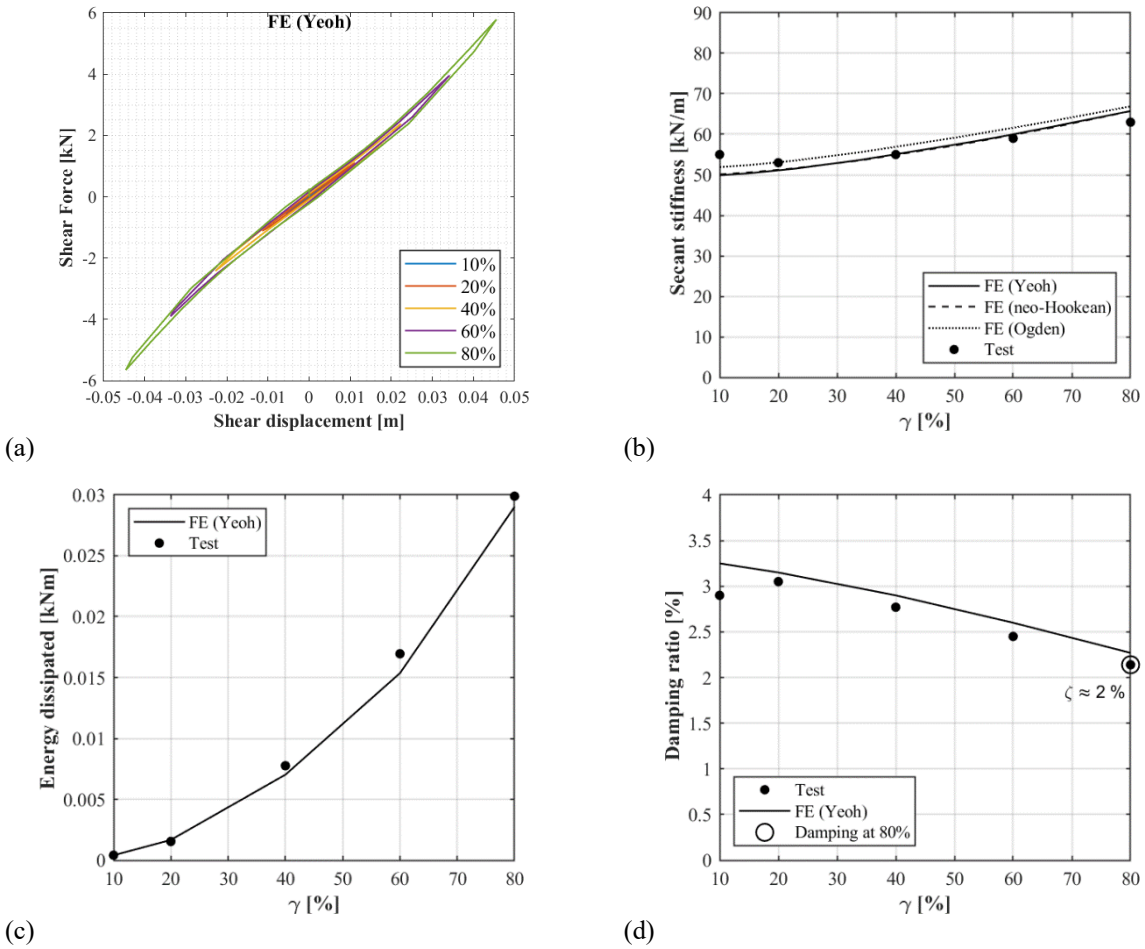

Fig. 11 –Cyclic behaviour of the bearing under different shear amplitudes with a static vertical displacement equivalent to a load of 19kN; comparison of experiment with hyperelastic FE augmented with Rayleigh damping (a) Hysteretic loops from the sinusoidal tests with amplitudes ranging from 10% up to 80% shear strain; (b) Secant shear stiffness-nominal shear strain relation; (c) Energy dissipated by the bearing, (d) Equivalent damping ratio at different levels of shear strain

2.3 Influence of axial compression on horizontal response and critical load estimation

The behaviour of LSF isolation bearings under shear loading is strongly influenced by the applied compression load. In particular, this load induces a significant reduction of the shear stiffness due to nonlinear geometrical effects (i.e., p-delta effects). However, in the case of LSF bearings the bulging of the rubber layers due to compression enhances the bearing stability by strongly increasing the tangent tilting stiffness of the individual bonded sandwiches [56]. In the case of bearings with high shape factor, the effect of the bulging on the tilting stiffness is expected to be negligible. The pressure also increases the damping capabilities under horizontal loading [23,48,57]. An analytical model capable of accurately describing all these effects in bearings for all possible values of shape factors has not been developed, yet. A simple mechanical model was developed in the past by Koh and Kelly [23,58] to describe the coupled vertical-shear response of elastomeric isolation bearings with high shape factor. This model was validated against some experimental results on bearings with values of S in the range 5-10. The dependency of horizontal stiffness on vertical stresses was studied also including large

displacements and non-linearity of rubber by other authors [24,59]. However, these theories are accurate only in the case of high shape factors and fail in providing a description of the behaviour of LSF bearings.

The 3D FE modelling strategy described in this study simulates with accuracy such shear-compression behaviour of LSF bearings. Fig. 12a shows the capability of the FE model to describe the sinusoidal tests performed at different compression levels for an 80% shear strain amplitude. Fig. 12b-c-d shows the results of the numerical analysis performed at different vertical loads and the comparison with the experimental results. Fig. 12b compares the estimates of the initial shear stiffness at zero shear displacement for increasing values of the applied vertical displacement according to the numerical FE models and the experimental results. In general, the horizontal stiffness reduces for increasing compression levels, attaining the critical condition of zero initial tangent stiffness for compressive loads higher than that considered experimentally. The variation with the compressive load of the energy dissipated (Fig. 12c) and of the equivalent damping ratio (Fig. 12d) are both well described by the Yeoh FE model together with Rayleigh damping.

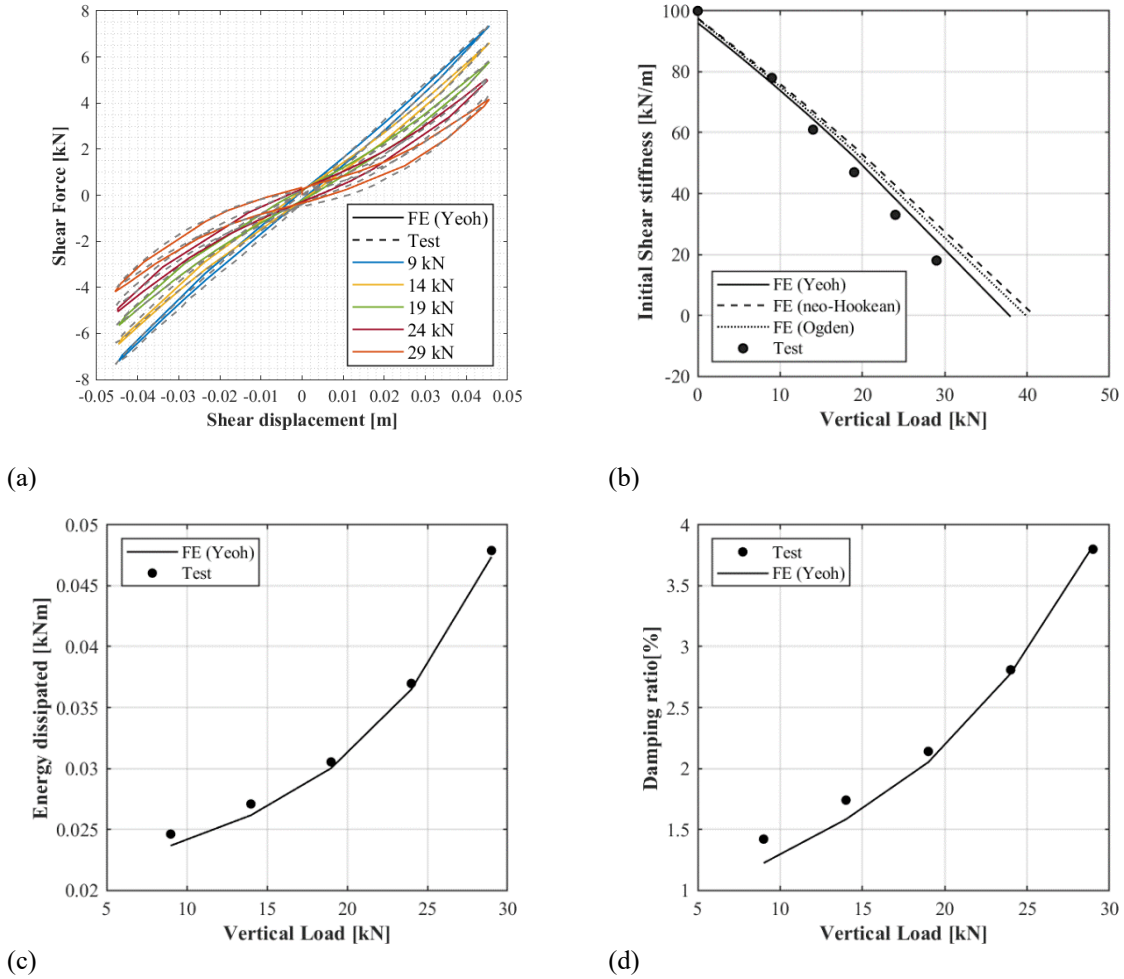

Fig. 12 – Cyclic behaviour of bearing under different compression levels with 80% shear strain (a) Hysteretic loops from the sinusoidal tests, (b) Shear stiffness vs vertical compression load, (c) Energy dissipated by the bearing, (d) Equivalent damping ratio

The maximum compressive load considered experimentally is 29kN as shown in Fig. 12b. However numerical analyses are also performed for higher compression levels to estimate the critical load and the corresponding axial deflection. It can be observed that the vertical deflections are significant, i.e. about 26% of the total rubber height, due to the compliance of the LSF bearing. Table 3 illustrates the numerical estimates of the critical load P_{cr} and the axial deflection d_{cr} according to the various constitutive laws considered in the numerical models. Reported in the same table is also the critical load estimated according to the theory of Koh and Kelly [23], which is only 19% of the values evaluated via the FEAs.

Table 3 Critical load estimated by Koh and Kelly and numerical estimates of critical load and corresponding axial deflection

Koh and Kelly	**FEA**					
	Ogden		**Yeoh**		**neo-Hookean**	
P_{cr}(kN)	P_{cr} (kN)	d_{cr} *(mm)*	P_{cr} (kN)	d_{cr} *(mm)*	P_{cr} (kN)	d_{cr} *(mm)*
7.4	40	15.69	39	15.02	41	15.19

In order to investigate the influence of the boundary conditions on the behaviour at large horizontal displacements, two quasi-static numerical analyses are carried out. The first one consists of the application of a constant axial load of 19kN and 39kN to the bearing, followed by a monotonically increasing horizontal displacement. In the second test, the bearing is subjected to a vertical displacement corresponding to a vertical compression of 19kN and 39kN, which is kept constant when the increasing horizontal displacement is applied. Fig. 13a illustrates how the two responses, in force-controlled and displacement-controlled mode, (and thus the horizontal initial stiffness) are coincident for low values of the horizontal displacement, whereas for increasing horizontal displacements the force-controlled test exhibits a softer response and attains a condition of zero horizontal tangent stiffness [60] as shown in Fig. 13b for 19kN axial load. In the case of fixed vertical displacement, the bearing exhibits a hardening behaviour in the horizontal direction, with the horizontal displacement resisted by a tensile load in the bearing. Eventually, the bearing would fail due to either cavitation or debonding between the rubber layer and the steel laminates. These results are very important, since they show that the test setup described in Section 2.1, which is cheaper and simpler than the one employed in other studies in the literature, is valid not only for model calibration and validation, but also for estimating the initial stiffness and buckling load of the bearings. It is worth observing that regardless the boundary conditions, the buckling load is attained at 39kN, according to the Yeoh numerical model.

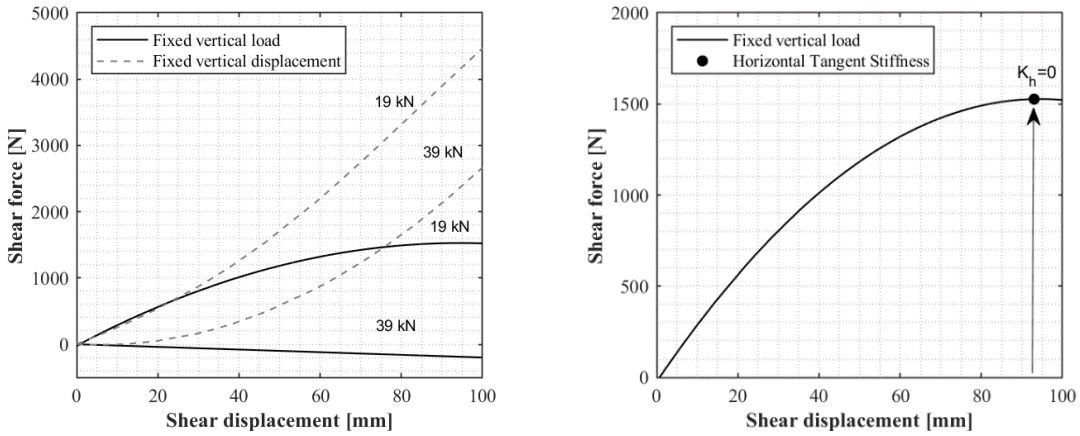

(a) (b)

Fig. 13 – Shear force-displacement behaviour (a) Force-controlled and displacement-controlled test results at 19kN and 39kN compression levels, (b) Schematic representation for stability limit at 19kN [60]

3. SHAKING TABLE TESTS

3.1 Prototype, Tests Description and Dynamic Identification

This subsection describes the shaking table tests carried out at the Department of Structures for Engineering and Architecture of University of Naples Federico II on a prototype base-isolated building with LSF bearings [18]. The superstructure is a one storey steel frame (Fig. 14) and it has a total height of 2900mm and plan dimensions of 2650x2150mm. The columns are fabricated by full penetration welding of four steel plates, have a box section 150x150x15mm, and they are connected to the base floor by means of a steel plate (610x450mm). The beams of the top floor are pinned to the columns and are hot-formed square hollow sections 120x120x12.5mm. The four perimetric beams at the base of the frame have HEM 160 profile. The bearings are identical to those tested at TARRC. The same mock-up has been recently used for bi-directional tests on recycled rubber and fibre-reinforced unbounded isolators [61,62].

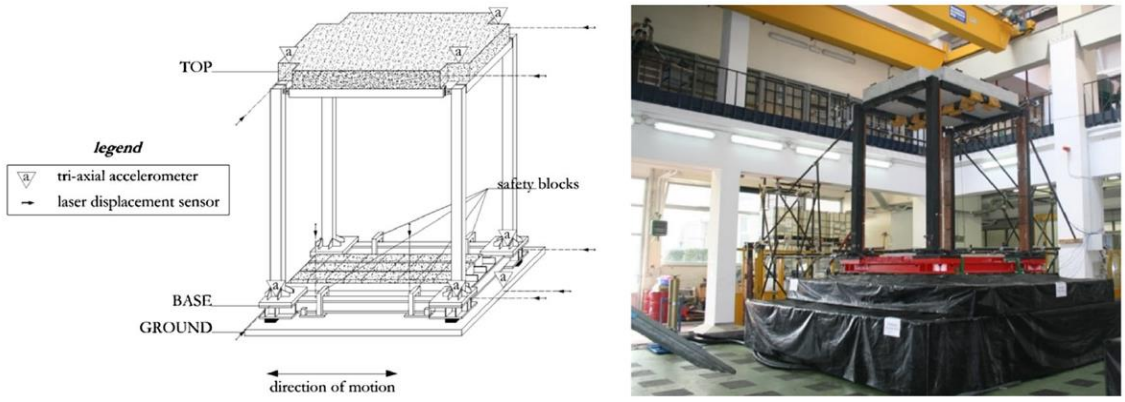

(a) (b)

Fig. 14 – (a) Cabinet projection of the prototype building and the instrumentation set-up, (b) view of the test frame of the shaking table at the DiST laboratory University of Naples Federico II [63]

Concrete blocks were added to the two levels to achieve a total mass M_{tot}= 7.7 tons. The total base floor mass is equivalent to 3.6 tons and the top floor mass is equal to 4.1 tons. Ground motions were applied along the direction in which the frame span is 2650 mm. The vibration period of the fixed-base structure is T_s=0.24 s. The isolation system of the scaled prototype was designed to achieve a nominal horizontal vibration period T_{is} = 0.92 s, estimated from an assumed value of the rubber shear modulus of 0.5MPa and considering the superstructure as rigid and the bearings as infinitely stiff in the vertical direction. Under these simplifying assumptions, the nominal isolation period can be expressed as $T_{is}=2\pi\sqrt{(M_{tot}/K_{is})}$, where $K_{is} \approx 4GA/nh$ is the total stiffness of the set of four bearings, each of rubber area A and total rubber thickness nh, in the horizontal direction. It is noteworthy that the system was designed considering a geometry scale factor of 1/3 and an elastic modulus scale factor of 1. Therefore, according to the dynamic similitude rule, the equivalent period of the full-scale structure is T_{fs}= 1.59 s, (i.e. $T_{fs}= \sqrt{3}T_{is}$).

Random vibration tests with white noise excitation were performed on the shaking table before seismic excitation tests to characterize dynamically the model structure and evaluate the modal parameters of the isolated system. In particular, the dynamic identification is performed using the recorded acceleration responses at both base and top level from two random input tests (i.e. Test 1, Test 2) that produced a peak horizontal displacement of the bearings of 7.44 mm and 16.33 mm, corresponding respectively to 13% and 29% of shear strain. Two common techniques have been used to calculate the modal parameters, namely the Stochastic Subspace Identification (SSI) [64] and Frequency Domain Decomposition (FDD) [65] methods. The difference between the two methods is that the latter calculation uses the output that excites the system, whereas the former only uses the input.

Table 4 summarizes the results of the application of these two methods, in terms of modal shapes, frequencies and damping ratios. It can be observed that the fundamental vibration period is higher than the value of 0.92s assumed for the design. This is due to the simplifications made at the design stage, namely the assumptions of a rigid superstructure, of rubber bearings infinitely stiff in the vertical direction, a shear modulus of rubber of 0.50MPa and neglecting the effect of the compressive load in reducing their shear stiffness. Using the initial bearing stiffness K_{is} evaluated in subsection 2.3 under the axial load of 19kN an isolation period $T_{is}=2\pi\sqrt{(M_{tot}/K_{is})}$ =1.21s is obtained, which is close to the experimental values.

Table 4 Dynamic identification from white noise tests on the isolated system.

	SSI				**FDD**			
	Mode 1		**Mode 2**		**Mode 1**		**Mode 2**	
	Test 1	**Test 2**	**Test 1**	**Test 2**	**Test 1**	**Test 2**	**Test 1**	**Test 2**

Mode shape	**Base**	0.893	0.898	-1	-1	0.895	0.899	-1	-1
	Top	1	1	0.708	0.746	1	1	0.792	0.782
Frequency [Hz]		0.83	0.81	3.7	3.78	0.78	0.78	3.71	3.71
Natural Period [s]		1.21	1.24	0.27	0.26	1.28	1.28	0.27	0.27
Damping Ratio		0.0752	0.0642	0.0797	0.0425	0.0605	0.0549	0.0605	0.0549

3.2 Advanced 3D Seismic Analysis

A FE model of the isolated structure is developed in Abaqus to evaluate the effect of the axial compliance of the bearings on the dynamic properties of the system, to simulate the shaking table tests, and to analyse the effect of variation of axial loads, during the motion, on the response of the bearings. Fig. 15a illustrates the developed model, which consists of only half of the total structure, due to symmetry. Beam elements (i.e. “wire elements” in Abaqus) are employed to describe the frame, whereas the same model described in the previous sections is used for the bearings. The global coordinates are defined as shown in Fig. 15, where the *z* axis is perpendicular to the x-y plane. The steel columns and beams of the frame are assumed to remain elastic, and thus are described by assigning a Young’s modulus of 210000MPa, a Poisson’s ratio of 0.3, and mass density of 7.8E-09 ton/mm^3. Rigid elements 180mm high are used between the columns and the bearings to simulate the actual height of the beams and slab at the base floor. In the FE-model, the upper surface of the rectangular plate is connected with the bottom node of the rigid element using a “coupling kinematic connection” (see Fig. 15b). Mass elements are added to describe the bottom and top floor weights. The total weight of the superstructure model including the base beam and the top and bottom floor masses is 3.85 ton, which is half of the total superstructure mass and corresponds to a vertical load of 19kN on each rubber bearing. The out-of-plane displacement along *z* and rotation about *x* of nodes on the *x-y* plane are restrained to account for symmetry conditions. Fig. 15a also illustrates the four nodes and the two degrees of freedom that have been considered for the calculation of the mode shapes: nodes 1-2 represent the isolation system whereas the superstructure is described by nodes 3-4.

Static analysis is first carried out under the self-weight of the system. Subsequently, an eigenvalue analysis is performed. Table 5 shows the natural periods and the mode-shapes correspondent to the horizontal and vertical displacement, denoted as $u_{x,i}$ and $u_{y,i}$, respectively, where *i* is the *i*-th node. The mode shapes and natural periods for the first two vibration modes associated with the horizontal displacement, exhibit a good agreement with the values obtained from system identification of the recorded data (Table 4). The fundamental period of the numerical model is higher than the isolation period T_{is}=1.21s obtained by disregarding the compliance of the bearings in the vertical direction and assuming rigidity of the superstructure, as expected. It is also slightly higher than the fundamental isolation period evaluated experimentally using SSI and FDD methods (respectively 1.21s and 1.28s).

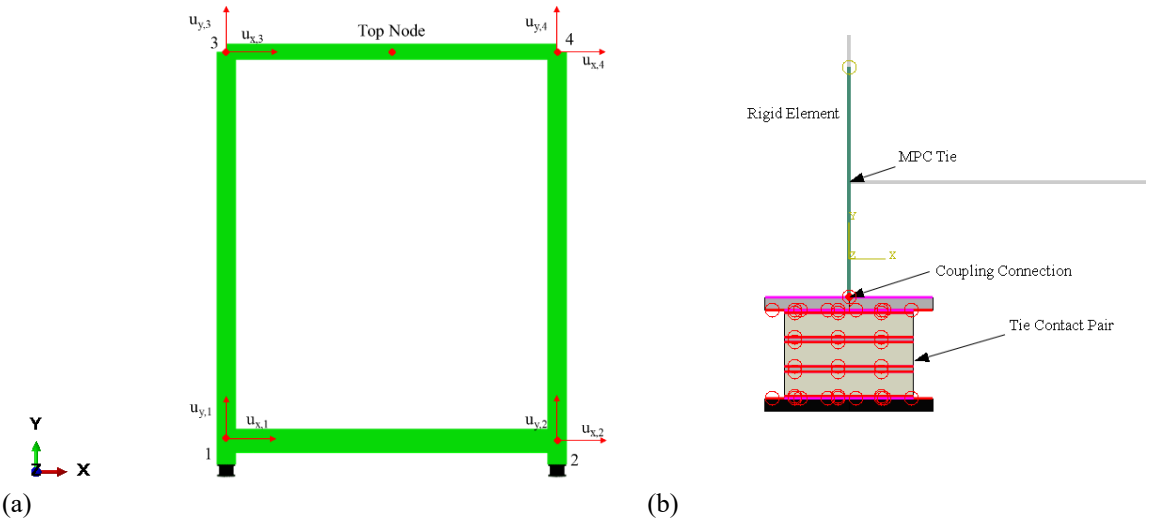

(a) (b)

Fig. 15 – (a) Finite element model of the isolated structure, (b) Contact details

Table 5 Abaqus FEA - Natural periods and mode shapes for base-isolated model

Mode			**First (Isolation mode)**	**Second**	**Third**
Natural Periods [s]			1.39	0.27	0.19
Natural Frequency [Hz]			0.72	3.70	5.26
Mode Shape	$u_{x,i}$	1	0.89	1.00	0.0003
		2	0.89	1.00	-0.0003
		3	1.00	-0.63	-0.0016
		4	1.00	-0.63	0.0016
	$u_{y,i}$	1	0.026	-0.379	1.00
		2	-0.026	0.379	1.00
		3	0.026	-0.379	1.00
		4	-0.026	0.379	1.00

Fig. 16 also illustrates the mode shapes for the first two modes. It is evident that the first dynamic mode of the isolated structure involves mainly a horizontal motion of the isolation system, with a slight in-phase rocking of the building, whereas the second mode involves strong antiphase motion but with significant deformation of the bearings in the vertical direction, with one bearing being compressed and the other extended by the rocking. Thus, some coupling is expected between the horizontal and vertical response of the bearings, even under the application of horizontal component of the earthquake [13]. It is noteworthy that the vibration periods of the first and second mode obtained by performing the eigenvalue analysis on the system not subjected to the static gravity loadings are equal respectively to 0.97s and 0.30s. Thus, the fundamental period increases by about 40% considering the effect of static loadings, whereas the period of the second mode decreases slightly by about 10%. This is due to the increase of axial stiffness of the bearings, which reduces the rocking component of vibration motion (Fig. 16b).

After application of the self-weight of the frame, dynamic implicit time-history analysis is carried out to simulate seismic response of the base-isolated frame under Bingol earthquake. Other seismic records were also considered in the experimental tests, but the response under this earthquake is the most interesting one since it is characterized by the largest displacement demands in the bearings among the various records and a condition close to instability.

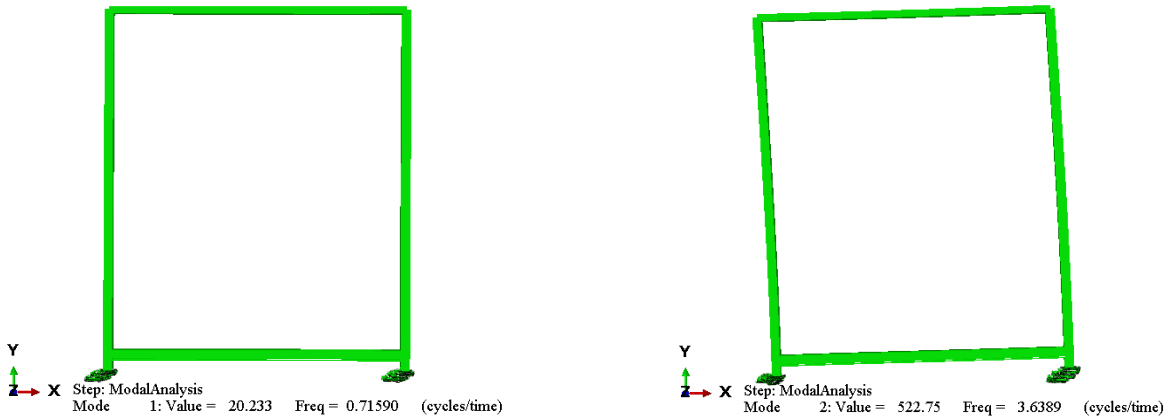

(a) (b)

Fig. 16 – Mode Shapes corresponding to (a) the first mode, and (b) the second mode.

It is noteworthy that the analyses are computationally very expensive, due to the high number of degrees of freedom, the use of a large displacement formulation and the bearings being in a highly deformed condition, and also approaching instability. Thus, more than 3 days are required on a medium-performance personal computer to run this analysis.

Fig. 17a shows the earthquake history imposed on the bottom of the bearing in the FE analysis. The initial time step of integration is 0.02 s, which is automatically reduced, if necessary. Fig. 17b-c-d show and compare the time histories of relative horizontal displacement of the bearing, interstorey drift (calculated as relative top-base displacement over interstorey height) and acceleration of the superstructure according to the experimental test [18] and the FE model.

The relative horizontal displacement of the bearing is the displacement of the top of the bearing with respect to the ground (that is the bottom of the bearing). The agreement between the two bearing responses (Fig. 17b) is quite good, up to approximately 10 sec, at which point the amplitude of the input ground motion decreases and the differences between the test and model becomes more significant. This may be due to the fact that the bearing model is more flexible than the actual bearing at low nominal shear strains (Fig. 11b). Moreover, higher discrepancies between the model and test results are observed for the superstructure acceleration and drift responses. This may also be due to the fact that the connection of the steel column to the base has some flexibility, while it is assumed to be rigid in the numerical model. This discrepancy is reflected in the shape of

mode 2, with the experimental modal shape characterised by higher superstructure deflections (0.708) compared to the numerical shape (0.63). It is noted that the oscillation period, measured as the distance between two consecutive displacement peaks, is equal to 1.38s (i.e., the value of the fundamental period from eigenvalue analysis) for small displacement amplitudes, and 1.5s for higher displacement amplitudes. This shows that at high amplitudes of deformation the bearing stiffness reduces significantly, as discussed more in detail below. Fig. 17e shows the rotation experienced by the base slab under seismic load, which is in phase with the bearing deflection and thus is induced by the deformation of the bearings in the vertical direction. Fig. 17f illustrates the contributions to the displacement response of the top node by the horizontal deflections of the bearings, the superstructure deflection, the rocking contribution of Fig. 17e and the sum of the three contributions. It can be observed that the displacements are all in phase (suggesting mode 1 of Fig. 16a predominates) and the top node response (see Fig. 15a) is dominated by the bearing deflection. This outcome is in agreement with relevant literature on 3D seismic isolation providing a major contribution of the rocking mode in case of vertical frequency lower than 1.0 Hz (i.e. approximately 30% of the second mode frequency in Table 5) [16],[66]. It can be noted in Fig. 17f that superstructure and rocking contribution time history are almost overlapping demonstrating that damage to non-structural components can be mainly due to the former component rather the latter, i.e. approximately 50% of total interstorey drift in Fig. 17c.

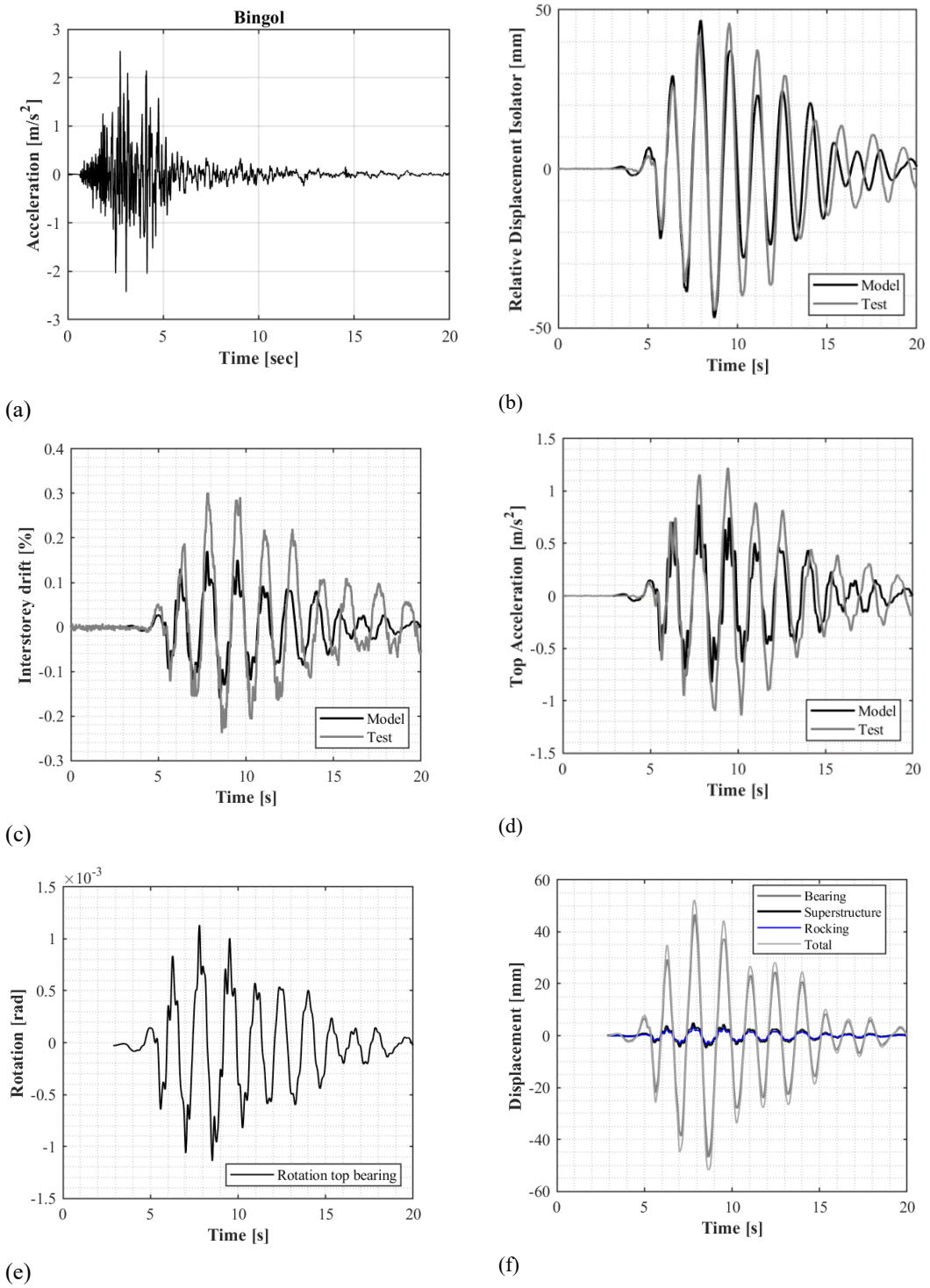

Fig. 17 – (a) Input ground motion: Bingol acceleration time history, (b) Relative Displacement Isolator time history, (c) Interstorey drift, (d) Acceleration at the top of the superstructure, (e) Rotation time history, (f) Time-history of the various contributions to the top node displacement.

Fig. 18 shows the bearing deformed shape and the corresponding shear strains and stresses observed at the time when the displacement response is the highest (i.e., 48 mm). It can be observed that the local shear strains vary significantly within the rubber and their values can be very different to the nominal one, which is 80%. Regarding the stresses distribution, local tensile stresses are developed within the bearing due to the bulging of the layers.

The Bingol earthquake involves highly non-linear behaviour in the bearing as well as coupling between the horizontal and vertical responses. In order to shed light into this aspect, Fig. 19a shows the time history of the vertical reaction for the left and right bearings of the isolated structure and Fig. 19b shows the variation of the vertical force with the horizontal displacement for the two bearings; the significance of rocking is evident from the inverse correlation between left and right bearings. It can be observed that the vertical forces exhibit a significant excursion, with values varying in the range between 16 kN and 24 kN. It is also interesting to observe that higher modes of vibration significantly affect the bearing responses in the vertical direction.

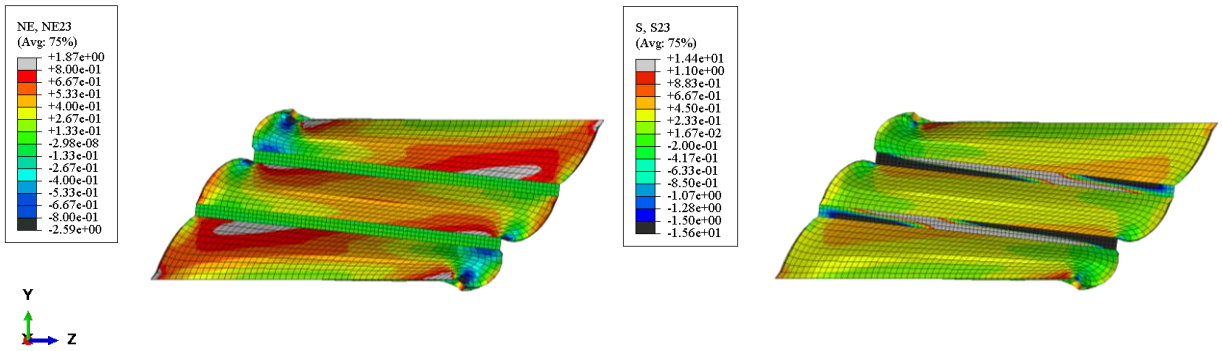

Fig. 18 – Contour plot of the shear strains (left) and stresses (right) component within the bearing

Fig. 19c-d illustrate respectively the time history of the horizontal reaction and horizontal force-displacement relationship for the left and right bearings. It can be observed that when the bearings are sheared to the positive horizontal direction, the vertical compression force in the left bearing reduces, while the one in the right bearing increases, while an opposite behaviour is observed in the opposite direction, as expected. When the compressive load increases, the horizontal tangent stiffness decreases, approaching a zero value for a vertical load of about 30kN as shown in Fig. 12b.

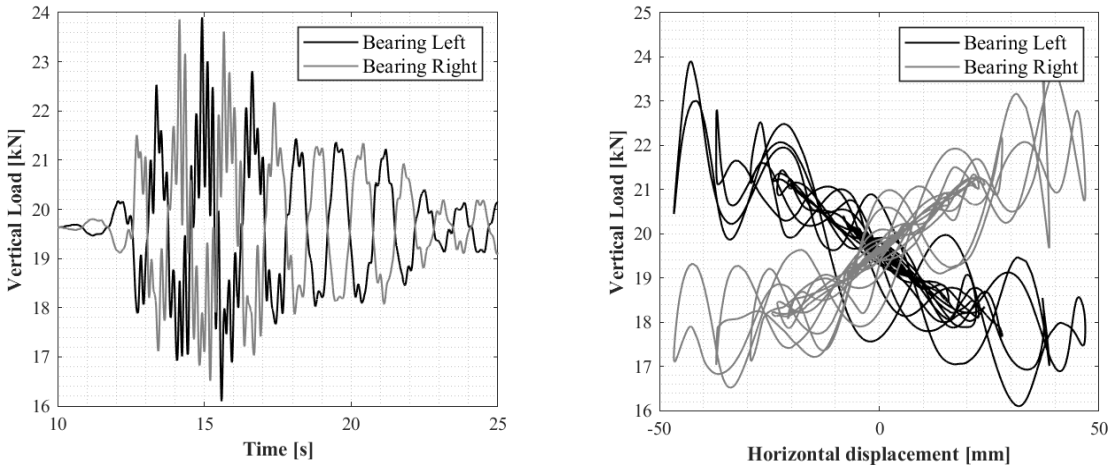

(a) (b)

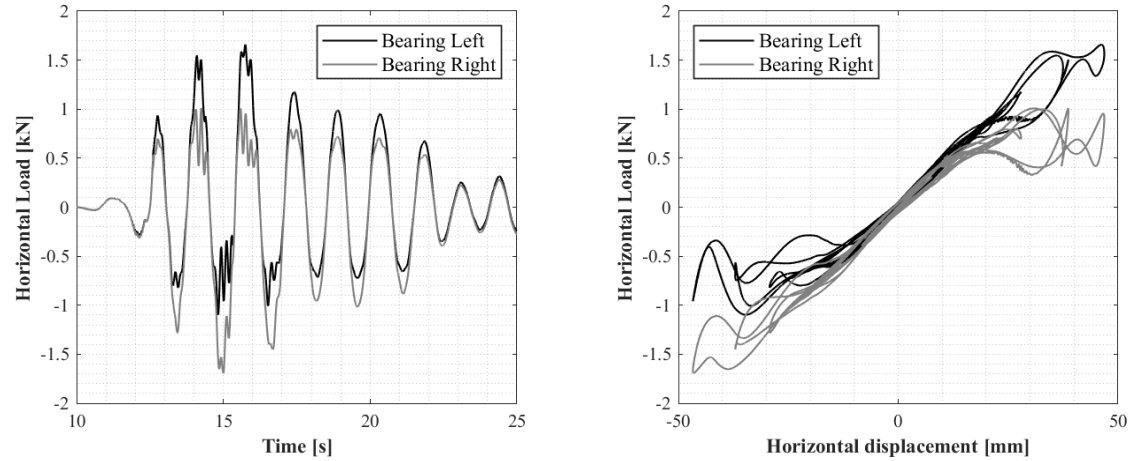

(c) (d)

Fig. 19 – a) Variation of vertical load with time, b) Vertical load-horizontal displacement behaviour, c) Variation of horizontal load with time, d) Horizontal load vs Horizontal displacement

CONCLUSIONS

This study investigates numerically the mechanical behaviour of elastomeric bearings with low shape factor (LSF) under compressive and shear loading, and the dynamic behaviour of a structure mounted on them. For this purpose, an unconventional test setup has been employed at Tun Abdul Razak Research Centre (TARRC), where LSF rubber bearings with low damping have been subjected first to compression, and then to shear loading under fixed compressive displacements. A three dimensional (3D) numerical model has been developed in Abaqus for simulating the experimental tests. Based on the results of these investigations, the following conclusion can be drawn:

These results are very important, since they show that the test setup described in Section 2.1, which is cheaper and simpler than the one employed in other studies in the literature, is valid not only for model calibration and validation, but also for estimating the initial stiffness and buckling load of the bearings.

- The 3D numerical model provided useful information in terms of local stress and strain in the rubber bearing due to the application of vertical load of 19kN and of 80% shear strain. Tensile stress and strain are concentrated along the bulging area when the bearing is subjected to the maximum compression load. Under maximum horizontal displacement, the contour plots show the formation of a compression strut, whereas tensile stresses are concentrated along the opposite diagonal.
- Hyperelastic material models, calibrated against material double-shear tests, can be used to accurately describe the complex nonlinear shear response of compressed LSF bearings. The neo-Hookean model provides a good fit for the shear rubber response up to nominal shear strains of 100% whereas the Yeoh

and Ogden hyperelastic material models are found to also describe properly the rubber material behaviour for larger nominal shear deformations. Moreover, when analyzing the local behaviour, which includes small regions of high strain, significant differences are observed between predictions of the neo-Hookean model and those of the Yeoh and Ogden models, which are larger than the differences observed in the global vertical and horizontal force-deflection responses.

- Analytical formulations such as the one developed by Koh and Kelly for simulating the behaviour of isolation bearings with high shape factors cannot be used for the LSF bearings considered in this study and underestimate significantly the critical load and the horizontal stiffness of the compressed bearings. On the other hand, the 3D numerical models provide accurate simulations of the sinusoidal tests performed at different compression levels, with satisfactory predictions of the effect of compression on both the horizontal stiffness and damping.

In the second part of the paper, shaking table tests carried out on a structure isolated on LSF bearings are simulated using the advanced 3D numerical model of the bearings. Based on the results of these analyses, it can be concluded that:

- The simulated modal properties and response of the isolators under a horizontal earthquake input are in very good agreement with the experimental results, whereas the response of the superstructure is slightly underestimated. In particular, the relative errors in terms of maximum absolute value of interstorey drift and acceleration at the top of the structure are of the order of 40% and 30%, respectively.
- The displacement response of the system is dominated by the deflection of the bearings, whereas the contribution of the superstructure flexibility and of the rocking of the base due to the vertical compliance of the bearings is significantly smaller despite the bearings are quite flexible vertically.
- The horizontal force-displacement relationship of the bearings is linear for shear deformations up to 30%, whereas for higher values a notable and rapid reduction of the tangent stiffness is observed due to the nonlinear geometrical effects.

A future study will investigate the performance and modeling of LSF bearings made with high damping rubber compounds, characterized by a more complex mechanical behaviour, which have been also the object of experimental investigations. Further numerical analyses and parametric studies will be carried out to evaluate the capability of the LSF bearings to provide full three-dimensional isolation, to investigate the coupling between the rocking response and the horizontal response and how the vertical compliance of the bearing influences the rocking behaviour. Finally, simplified LSF bearing device models will be developed and

implemented in nonlinear seismic analysis codes such as OpenSees and SAP2000, allowing to perform more extensive analyses of the seismic response of structures mounted on LSF bearing.

ACKNOWLEDGEMENTS

Thanks are due for support given by Prof. Giorgio Serino and Fabrizia Cilento who provided data from experimental campaign carried out at the laboratories of TARRC and Department of Structures for Engineering and Architecture of University of Naples Federico II. The authors are also grateful to Giovanni Cuomo and Robert Picken who assisted with the bearing manufacturing and shaking table tests.

FUNDING

This research did not receive any specific grant from funding agencies in the public, commercial, or not-for-profit sectors.

REFERENCES

[1] Konstantinidis D., Kelly J. Mechanics of Rubber Bearings for Seismic and Vibration Isolation. 2011 Hoboken, N.J.: Wiley.

[2] Constantinou M., Kartoum A., Kelly J. Analysis of compression of hollow circular elastomeric bearings. *Engineering Structures.* 1992;14(2):103-111. doi:10.1016/0141-0296(92)90036-p

[3] Montuori G., Mele E., Marrazzo G., Brandonisio G., De Luca A. Stability issues and pressure–shear interaction in elastomeric bearings: the primary role of the secondary shape factor. *Bulletin of Earthquake Engineering*. 2015;14(2):569-597. doi:10.1007/s10518-015-9819-x

[4] Derham C., Kelly J., Thomas A.G., Nonlinear natural rubber bearings for seismic isolation,Nuclear Engineering and Design, 84(3), 417-428. 1985. https://doi.org/10.1016/0029-5493(85)90258-4.

[5] Kelly, J., and Niel C. Van Engelen. Fiber-reinforced elastomeric bearings for vibration isolation. *Journal of Vibration and Acoustics.* 2016; 138.1: 011015.

[6] Yenidogan C. Earthquake-Resilient Design of Seismically Isolated Buildings: A Review of Technology. *Vibration*. 2021; 4(3):602-647. https://doi.org/10.3390/vibration4030035

[7] Kelly J. Base Isolation in Japan, 1988. Berkeley, Calif.: Earthquake Engineering Research Centre, College of Engineering, University of California.

[8] Aiken I, Kelly J, Tajirian F. Mechanics of Low Shape Factor Elastomeric Seismic Isolation Bearings. 1989 Berkeley, Calif.: Earthquake Engineering Research Centre, College of Engineering, University of California, Berkeley.

[9] Kelly, J. Analysis of fiber-reinforced elastomeric isolators. *Journal of Seismology and Earthquake Engineering.* 1999; 2.1. 19-34

[10] Thuyet, Van Ngo, S. K. Deb, and A. Dutta. Mitigation of seismic vulnerability of prototype low-rise masonry building using U-FREIs. *Journal of Performance of Constructed Facilities*. 2018; 32.2: 04017136.

[11] Losanno D., Calabrese A., Madera Sierra I.E., Spizzuoco M., Marulanda J., Thomson P., Serino G. Recycled Versus Natural-Rubber Fiber-Reinforced Bearings for Base Isolation: Review of the Experimental Findings, *Journal of Earthquake Engineering*. 2020; DOI 10.1080/13632469.2020.1748764

[12] Losanno D., Madera Sierra I.E., Spizzuoco M., Marulanda J., Thomson P. Experimental assessment and analytical modeling of novel fiber-reinforced isolators in unbounded configuration, *Composite Structures.* 2019; 212, 66-82

[13] Kelly J., Lee J.J. Vertical Flexibility in Isolation Systems. *Civil Engineering Research Journal*. 2018;4(1). doi:10.19080/cerj.2018.04.555629

[14] Warn G, Vu B. Exploring the low shape factor concept to achieve threedimensional seismic isolation. In: *Recent Innovations And Application Of Passive Seismic Control*. Chicago, Illinois, United States: American Society of Civil Engineers; 2012:1-11. https://ascelibrary.org/doi/10.1061/9780784412374.001.

[15] Yabana S, Matsuda A. Mechanical properties of laminated rubber bearings for three-dimensional seismic isolation. In: *Proceedings of the 12th WCEE*, 2000, New Zealand.

[16] Zhou Z, Wong J, Mahin S. Potentiality of Using Vertical and Three-Dimensional Isolation Systems in Nuclear Structures. *Nuclear Engineering and Technology*. 48, 5, 2016, 1237-1251.

[17] Okamura S, Kamishima Y, Negishi K, Sakamoto Y, Kitamura S, Kotake S. Seismic Isolation Design for JSFR. J*ournal of Nuclear Science and Technology*. 2011 48:4, 688-692, DOI: 10.1080/18811248.2011.9711750

[18] Cilento F, Vitale R, Spizzuoco M, Serino G, Muhr A. Analysis of the Experimental Behaviour of Low Shape Factor Isolation Rubber Bearings by Shaking Table Investigation. In: *XVII Convegno Anidis*. 2017:21-30.

[19] Tubaldi E, Mitoulis S, Ahmadi H, Muhr A. A parametric study on the axial behaviour of elastomeric isolators in multi-span bridges subjected to horizontal seismic excitations. *Bulletin of Earthquake Engineering*. 2016;14(4):1285-1310. doi:10.1007/s10518-016-9876-9

[20] Kalfas K, Mitoulis S, Katakalos K. Numerical study on the response of steel-laminated elastomeric bearings subjected to variable axial loads and development of local tensile stresses. *Engineering Structures*. 2017;134:346-357. doi:10.1016/j.engstruct.2016.12.015

[21] Kikuchi M, Aiken I. An analytical hysteresis model for elastomeric seismic isolation bearings. *Earthq Eng Struct Dyn*. 1997;26(2):215-231. doi:10.1002/(sici)1096-9845(199702)26:2<215::aid-eqe640>3.0.co;2-9

[22] Kumar M, Whittaker A, Constantinou M. An advanced numerical model of elastomeric seismic isolation bearings. *Earthq Eng Struct Dyn*. 2014;43(13):1955-1974. doi:10.1002/eqe.2431

[23] Koh CG, Kelly J. Modeling of Seismic Isolation Bearings Including Shear Deformation and Stability Effects. ASME. *Appl. Mech. Rev*. November 1989; 42(11S): S113–S120. https://doi.org/10.1115/1.3152379

[24] Nagarajaiah S, Ferrell K. Stability of elastomeric seismic isolation bearings. *J Struct Eng (N Y)*. 1999;125(9):946-954.

[25] Kumar, M., Whittaker, A., and Constantinou, M. (2014). "An advanced numerical model of elastomeric seismic isolation bearings." Earthquake Engineering & Structural Dynamics, 43(13), 1955-1974.

[26] Kumar, M., and Whittaker, A. (2018). "Cross-platform implementation, verification and validation of advanced mathematical models of elastomeric seismic isolation bearings." Engineering Structures, 175, 926-943.

[27] Grant D, Fenves G, Whittaker A. Bidirectional modelling of high-damping rubber bearings. *Journal of Earthquake Engineering*. 2004;8(sup001):161-185. doi:10.1080/13632460409350524

[28] Tubaldi E, Ragni L, Dall'Asta A, Ahmadi H, Muhr A. Stress softening behaviour of HDNR bearings: modelling and influence on the seismic response of isolated structures. *Earthq Eng Struct Dyn*. 2017. doi:10.1002/eqe.2897

[29] Cardone D, Flora A, Gesualdi G. Inelastic response of RC frame buildings with seismic isolation. *Earthq Eng Struct Dyn*. 2012;42(6):871-889. doi:10.1002/eqe.2250

[30] Tubaldi, E., Mitoulis, S. A., & Ahmadi, H. (2018). Comparison of different models for high damping rubber bearings in seismically isolated bridges. *Soil Dynamics and Earthquake Engineering*, *104*, 329-345.

[31] Ragni, L., D. Cardone, Nadia Conte, A. Dall'Asta, A. Di Cesare, A. Flora, G. Leccese, F. Micozzi, and C. Ponzo. "Modelling and seismic response analysis of Italian code-conforming base-isolated buildings." Journal of Earthquake Engineering 22, no. sup2 (2018): 198-230.

[32] Stanton JF, Scroggins G, Taylor AW, Roeder CW. Stability of laminated elastomeric bearings. *J Eng Mech*. 1990;116(6):1351-1371.

[33] Roeder CW, Stanton JF. Design of laminated elastomeric bridge bearings. In: *Bridge Engineering Conference, 3rd, 1991, Denver, Colorado, USA*; 1991.

[34] R.A. Schapery. Elastomeric bearing sizing analysis Part 2: Flat and cylindrical bearings. *International*

Journal of Solids and Structures. vol 152–153, 2018, 140-150. ISSN 0020-7683,https://doi.org/10.1016/j.ijsolstr.2018.07.007.

[35] R.A. Schapery. Shim analysis for spherical elastomeric bearings. *International Journal of Solids and Structures*. 144–145,2018, 276-288. ISSN 0020-7683, https://doi.org/10.1016/j.ijsolstr.2018.05.013.

[36] AH Muhr. Lateral stiffness of rubber mounts under finite axial deformation. In: Constitutive Model for *Rubber X - Proceeding of the European Conference on Constitutive Model for Rubber*, ECCMR X. 2017. pp. 153– 158.

[37] Gu, Z., Lei, Y., Qian, W., Xiang, Z., Hao, F., & Wang, Y. (2021). An Experimental Study on the Mechanical Properties of a High Damping Rubber Bearing with Low Shape Factor. *Applied Sciences*, *11*(21), 10059

[38] Ren, X., Lu, W., Zhu, Y., He, Y., & Li, T. (2020). Compressive behavior of low shape factor lead-rubber bearings: Full-scale testing and numerical modeling. *Engineering Structures*, *209*, 110030

[39] DassaultSystèmes. ABAQUS/CAE 6.13user's Manual. Abaqus Ver. 6.13 Documentation, Providence, RI; 2018

[40] Ohsaki M, Miyamura T, Kohiyama M, Yamashita T, Yamamoto M, Nakamura N. Finite-element analysis of laminated rubber bearing of building frame under seismic excitation. *Earthq Eng Struct Dyn.* 2015, 44: 1881– 1898. doi: 10.1002/eqe.2570.

[41] Saidou A., Gauron O., Busson A., Paultre P. High-order finite element model of bridge rubber bearings for the prediction of buckling and shear failure. *Engineering Structures*, 240, 2021, 0141-0296, https://doi.org/10.1016/j.engstruct.2021.112314.

[42] Ragni L, Tubaldi E, Dall'Asta A, Ahmadi H, Muhr A. Biaxial shear behaviour of HDNR with Mullins effect and deformation-induced anisotropy. *Engineering Structures*. 2018;154:78-92.

[43] Chopra AK. Dynamics of Structures: Theory and Applications to Earthquake Engineering. 2012. Upper Saddle River, N.J.: Prentice Hall.

[44] Cuomo G. Design, Development And Experimental Validation Of Multilayer Modular Laminated Natural Rubber Isolators. Naples: University of Naples Federico II ; 2014.

[45] Gough J, Muhr AH. Initiation of failure of rubber close to bondlines. *Proc. International Rubber Conference*. 2005, Maastricht. IOM Communications Ltd, London, 165-174.

[46] ID Aiken, JM Kelly, PW Clark, K Tamura, M Kikuchi, T Itoh. Experimental studies of mechanical characteristics of three types of seismic isolation bearings. In: *10th World Conference on Earthquake Engineering*. 1992.

[47] TJ Pond, AG Thomas. The mechanics of laminated rubber bearings. *Journal of Natural Rubber Research*. 1993;8(4),260-274.

[48] Thomas AG. The Design of Laminated Bearings I. *Proceeding Conf. NR Earthq. Prot. Build.* 1982; 229–246.

[49] Raithel A., Serino G. Stabilità e Comportamento Post-Critico degli Isolatore Elastomerici Armati, 6° Convegno Nazionale L'Ingegneria Sismica in Italia, 13- 15 Ottobre, 1993. Perugia.

[50] International Atomic Energy Agency, Seismic Isolation Systems for Nuclear Installations, IAEA-TECDOC-1905, IAEA, Vienna (2020).

[51] Ogden RW. Non-Linear Elastic Deformations. 1984. Dover Civil and Mechanical Engineering.

[52] Rivlin RS. Large Elastic Deformations. In: Collected Papers of R.S. Rivlin. Springer New York; 1997:318-351.

[53] Gregory IH, Muhr AH. Stiffness and fracture analysis of bonded rubber blocks in simple shear. In: *Boast D, Coveney VA (eds) Finite Element Analysis of Elastomers*. Professional Engineering, London. 1999; p 265

[54] Ahmadi HR, Kingston JGR, Muhr AH. Dynamic properties of filled rubber — part I: Simple model, experimental data and simulated results. *Rubber Chem Technol*. 2008;81(1):1-18.

[55] Kelly, J.M. (1997). Behavior of Multilayered Bearings Under Compression and Bending. In: Earthquake-Resistant Design with Rubber. Springer, London. https://doi.org/10.1007/978-1-4471-0971-6_7

[56] Gent AN. Elastic stability of rubber compression springs. *J Mech Eng Sci*. 1964; 6(4):318-326

[57] Goodchild IR, Muhr AH, Thomas AG. The lateral stiffness and damping of a stretched rubber beam. *Plast Rubber Compos*. 2018;47(4):176-186.

[58] Koh CG, Kelly J. A simple mechanical model for elastomeric bearings used in base isolation. *Int J Mech Sci*. 1988;30(12):933-943.

[59] Buckle I, Nagarajaiah S, Ferrell K. Stability of elastomeric isolation bearings: Experimental study. *J Struct Eng (N Y)*. 2002;128(1):3-11.

[60] Sanchez J, Masroor A, Mosqueda G, Ryan K. Static and dynamic stability of elastomeric bearings for seismic protection of structures. *Journal of Structural Engineering.* 2013;139; 1149-1159.

[61] Losanno D, Spizzuoco M, Calabrese A. Bidirectional shaking-table tests of unbonded recycled-rubber fiber-reinforced bearings (RR-FRBs). *Struct Contr Health Monit*. 2019;26(9):e2386.

[62] Losanno D, Madera Sierra IE, Spizzuoco M, Marulanda J, Thomson P. Experimental performance of unbonded polyester and carbon fiber reinforced elastomeric isolators under bidirectional seismic

excitation. *Engineering Structures*. 2020;209(110003):110003.

[63] Calabrese A, Spizzuoco M, Serino G, Della Corte G, Maddaloni G. Shaking table investigation of a novel, low-cost, base isolation technology using recycled rubber. *Struct Contr Health Monit*. 2015;22(1):107-122.

[64] Van Overschee P, De Moor BL. Subspace Identification for Linear Systems: Theory — Implementation — Applications. 1996th ed. Springer; 2012. Accessed March 15, 2021. https://www.springer.com/gp/book/9781461380610.

[65] Brincker R, Zhang L, Andersen P. Modal identification of output-only systems using frequency domain decomposition. *Smart Mater Struct*. 2001;10(3):441-445.

[66] Wang T., Wang F. Three-dimensional base-isolation system using thick rubber bearings. *Proc. SPIE 8341, Active and Passive Smart Structures and Integrated Systems*. 2012; 83412K (27 March 2012); https://doi.org/10.1117/12.916965].

WEB REFERENCES

[67] https://www.lord.com/emea/sites/emea/files/DS3901E_Chemosil211UK.pdf

[68] https://www.henkel-adhesives.com/uk/en/product/retaining-compounds/loctite_638.html